Title
EXTENSOMETER PERFORMANCE DURING HEATER EXPERIMENTS AT STRIPA

Author
DuBois, A.O.

Publication Date
1981-10-01

LBL-13531
SAC-50
UC-70

SWEDISH-AMERICAN COOPERATIVE PROGRAM ON RADIOACTIVE WASTE STORAGE IN MINED CAVERNS IN CRYSTALLINE ROCK

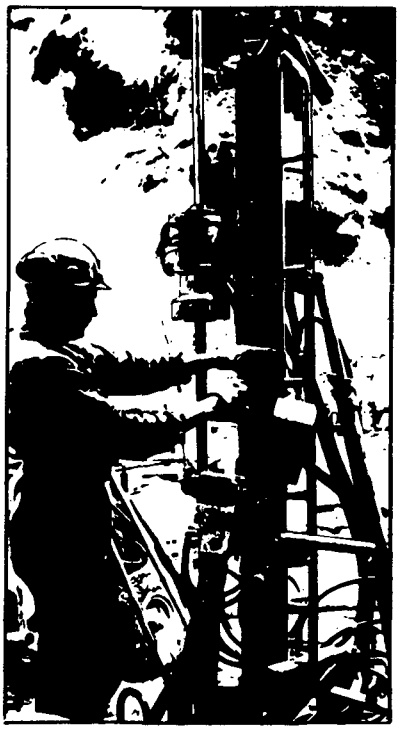

Technical Information Report No. 50

EXTENSOMETER PERFORMANCE DURING HEATER EXPERIMENTS AT STRIPA

A.O. DuBois, M. Hood, E.P. Binnall, and L. Andersson

Lawrence Berkeley Laboratory
University of California
Berkeley, California 94720

October 1981

A Joint Project of

Swedish Nuclear Fuel Supply Co.
Fack 10240 Stockholm, Sweden

Operated for the Swedish
Nuclear Power Utility Industry

Lawrence Berkeley Laboratory
Earth Sciences Division
University of California
Berkeley, California 94720, USA

Operated for the U.S. Department of
Energy under Contract DE-AC03-76SF00098

DISCLAIMER

LBL-13531
SAC-50
UC-70

EXTENSOMETER PERFORMANCE DURING HEATER EXPERIMENTS AT STRIPA

A. O. DuBois, M. Hood, E. P. Binnall, and L. Andersson

Earth Sciences Division
Lawrence Berkeley Laboratory
University of California
Berkeley, California 94720

October, 1981

This work was supported by the Assistant Secretary for Nuclear Energy, Office of Civilian Waste Management of the U. S. Department of Energy under Contract DE-AC03-76SF00098. Funding for this project is administered by the Office of Crystalline Repository Development at Battelle Memorial Institute.

PREFACE

This report is one of a series documenting the results of the Swedish-American cooperative research program in which the cooperating scientists explore the geological, geophysical, hydrological, geochemical, and structural effects anticipated from the use of a large crystalline rock mass as a geologic repository for nuclear waste. This program has been sponsored by the Swedish Nuclear Power Utilities through the Swedish Nuclear Fuel Supply Company (SKBF), and the U.S. Department of Energy (DOE) through the Lawrence Berkeley Laboratory.

The principal investigators are L.B. Nilsson and O. Degerman for SKBF, and N.G.W. Cook, P.A. Witherspoon, and J.E. Gale for LBL. Other participants will appear as authors of the individual reports.

Previous technical reports in this series are listed below.

1. Swedish-American Cooperative Program on Radioactive Waste Storage in Mined Caverns by P.A. Witherspoon and O. Degerman. (LBL-7049, SAC-01).

2. Large Scale Permeability Test of the Granite in the Stripa Mine and Thermal Conductivity Test by Lars Lundstrom and Haken Stille. (LBL-7052, SAC-02).

3. The Mechanical Properties of the Stripa Granite by Graham Swan. (LBL-7074, SAC-03).

4. Stress Measurements in the Stripa Granite by Hans Carlsson. (LBL-7078, SAC-04).

5. Borehole Drilling and Related Activities at the Stripa Mine by P.J. Kurfurst, T. Hugo-Persson, and G. Rudolph. (LBL-7080, SAC-05).

6. A Pilot Heater Test in the Stripa Granite by Hans Carlsson. (LBL-7086, SAC-06).

7. An Analysis of Measured Values for the State of Stress in the Earth's Crust by Dennis B. Jamison and Neville G.W. Cook. (LBL-7071, SAC-07).

8. Mining Methods Used in the Underground Tunnels and Test Rooms at Stripa by B. Andersson and P.A. Halen. (LBL-7081, SAC-08).

9. Theoretical Temperature Fields for the Stripa Heater Project by T. Chan, Neville G.W. Cook, and C.F. Tsang. (LBL-7082, SAC-09).

10. Mechanical and Thermal Design Considerations for Radioactive Waste Repositories in Hard Rock. Part I: An Appraisal of Hard Rock for Potential Underground Repositories of Radioactive Waste by N.G.W. Cook; Part II: In Situ Heating Experiments in Hard Rock: Their Objectives and Design by N.G.W. Cook and P.A. Witherspoon. (LBL-7073, SAC-10).

11. Full-Scale and Time-Scale Heating Experiments at Stripa: Preliminary Results by N.G.W. Cook and M. Hood. (LBL-7072, SAC-11).

12. Geochemistry and Isotope Hydrology of Groundwaters in the Stripa Granite: Results and Preliminary Interpretation by P. Fritz, J.F. Barker, and J.E. Gale. (LBL-8285, SAC-12).

13. Electrical Heaters for Thermo-Mechanical Tests at the Stripa Mine by R.H. Burleigh, E.P. Binnall, A.O. DuBois, D.O. Norgren, and A.R. Ortiz. (LBL-7063, SAC-13).

14. Data Acquisition, Handling, and Display for the Heater Experiments at Stripa by Maurice B. McEvoy. (LBL-7063, SAC-14).

15. An Approach to the Fracture Hydrology at Stripa: Preliminary Results by J.E. Gale and P.A. Witherspoon. (LBL-7079, SAC-15).

16. Preliminary Report on Geophysical and Mechanical Borehole Measurements at Stripa by P. Nelson, B. Paulsson, R. Rachiele, L. Andersson, T. Schrauf, W. Hustrulid, O. Duran, and K.A. Magnussen. (LBL-8280, SAC-16).

17. Observations of a Potential Size-Effect in Experimental Determination of the Hydraulic Properties of Fractures by P.A. Witherspoon, C.H. Amick, J.E. Gale, and K. Iwai. (LBL-8571, SAC-17).

18. Rock Mass Characterization for Storage in Nucler Waste in Granite by P.A. Witherspoon, P. Nelson, T. Doe, R. Thorpe, B. Paulsson, J.E. Gale, and C. Forster. (LBL-8570, SAC-18).

19. Fracture Detection in Crystalline Rock Using Ultrasonic Shear Waves by K.H. Waters, S.P. Palmer, and W.F. Farrell. (LBL-7051, SAC-19).

20. Characterization of Discontinuities in the Stripa Granite--Time Scale Heater Experiment by R. Thorpe. (LBL-7083, SAC-20).

21. Geology and Fracture System at Stripa by A. Okliewicz, J.E. Gale, R. Thorpe, and B. Paulsson. (LBL-8907, SAC-21).

22. Calculated Thermally Induced Displacements and Stresses for Heater Experiements at Stripa by T. Chan and N.G.W. Cook. (LBL-7061, SAC-22).

23. Validity of Cubic Law for Fluid Flow in a Deformable Rock Fracture by P.A. Witherspoon, J. Wang, K. Iwai, and J.E. Gale. (LBL-9557, SAC-23).

24. Determination of In-Situ Thermal Properties of Stripa Granite from Temperature Measurements in the Full-Scale Heater Experiments: Methods and Primary Results by J. Jeffry, T. Chan, N.G.W. Cook and P.A. Witherspoon. (LBL-8424, SAC-24).

25. Instrumentation Evaluation, Calibration, and Installation for Heater Tests Simulating Nuclear Waste in Crystalline Rock, Sweden by T. Schrauf, H. Pratt, E. Simonson, W. Hustrulid, P. Nelson, A. DuBois, E. Binnall, and R. Haught. (LBL-8313, SAC-25)

26. Part I: Some Results From a Field Investigation of Thermo-Mechanical Loading of a Rock Mass When Heater Canisters are Emplaced in the Rock by M. Hood. Part II: The Application of Field Data from Heater Experiments Conducted at Stripa, Sweden for Repository Design by M. Hood, H. Carlsson, and P.H. Nelson. (LBL-9392, SAC-26).

27. Progress with Field Investigations at Stripa by P.A. Witherspoon, N.G.W. Cook, and J.E. Gale (LBL-10559, SAC-27).

28. A Laboratory Assessment of the Use of Borehole Pressure Transients to Measure the Permeability of Fractured Rock Masses by C.B. Forster and J.E. Gale. (LBL-8674, SAC-28).

29. Thermal and Thermomechanical Data for In Situ Heater Experiments at Stripa, Sweden by T. Chan, E. Binnall, P. Nelson, O. Wan, C. Weaver, K. Ang, J. Braley, and M. McEvoy. (LBL-11477, SAC-29).

30. The Effect of Radon Transport in Groundwater Upon Gamma Ray Borehole Logs by P.H. Nelson, R. Rachiele, and A. Smith. (LBL-11180, SAC-30).

31. Strength and Permeability Tests on Ultra-Large Stripa Granite Core by R. Thorpe, D.J. Watkins, W.E. Ralph, R. Hsu, and S. Flexser. (LBL-11203, SAC-31).

32. Ultrasonic and Acoustic Emission Results from the Stripa Heater Experiments. Part I: A Cross-Hole Investigation of a Rock Mass Subjected to Heating by B.N.P. Paulsson and M.S. King. Part II: Acoustic Emission Monitoring During Cool-Down of the Stripa Heater Experiment by R. Rachiele. (LBL-10975, SAC-32).

33. Numerical Modeling to Assess Possible Influence of the Mine Openings on Far-Field In Situ Stress Measurements at Stripa by T. Chan, V. Guvanasen, and N. Littlestone (LBL-12469, SAC-33).

34. A Field Assessment of the Use of Borehole Pressure Transients to Measure the Permeability of Fractured Rock Masses by C.B. Forster and J.E. Gale. (LBL-11829, SAC-34).

35. Water Inflow into Boreholes During the Stripa Experiments by P.H. Nelson, R. Rachiele, J.S. Remer and H.S. Carlsson. (LBL-12547, SAC-35).

36. Petrology and Radiogeology of the Stripa Pluton by H. Wollenberg, S. Flexser, and L. Andersson. (LBL-11654, SAC-36).

37. Geohydrological Data from the Macopermeability Experiment at Stripa, Sweden by C.R. Wilson, J.C.S. Long, R.M. Galbraith, K. Karasaki, H.K. Endo, A.O. DuBois, M.J. McPherson, and G. Ramqvist. (LBL-12520, SAC-37).

38. Characterization of Discontinuities in the Stripa Granite--Full-Scale Heater Experiments by B.N.P. Paulsson, P.H. Nelson, and P.J. Kurfurst. (LBL-9063, SAC-38).

39. Application of Borehole Geophysics at an Experimental Waste Storage Site by P.H. Nelson, K.A. Magnusson, and R. Rachiele. (LBL-11982, SAC-39).

40. Laboratory Investigations of Thermomechanical Properties of Stripa Granite by L. Myer and R. Rachiele. (LBL-13435, SAC-40)

41. Petrologic Changes and Damage in the Stripa Quartz Monzonite in Response to Heater Tests by S. Flexser, H. Wollenberg, and D.E. Wedge. (LBL-14929, SAC-41).

42. Fracture Mapping in the Ventilation Drift at Stripa: Procedures and Results by A. Rouleau, J.E. Gale, and J. Baleshta. (LBL-13071, SAC-42).

43. Thermal Analysis of the Stripa Heater Test Data from the Full Scale Drift by I. Javandel and P.A. Witherspoon. (LBL-13217, SAC-43).

44. In Situ Stress Measurements at the Stripa Mine, Sweden by T.W. Doe, K. Ingevald, L. Strindell, B. Leijon, W. Hustrulid, A. Tarikka, M. Holmberg, E. Majer, and H. Carlsson. (LBL-15009, SAC-44).

45. Fracture Detection in Crystalline Rock Using Ultrasonic Reflection Techniques by S.P. Palmer. (LBL-16347, SAC-45).

46. Fracture and Hydrology Data from Field Studies at Stripa, Sweden by J.E. Gale. (LBL-13101, SAC-46).

47. Equipment Design, Installation, and Operation for the Macropermeability Experiment at Stripa, Sweden by R.M. Galbraith, C.R. Wilson, A.O. DuBois, S.A. Lundgren, M.J. McPherson and G.W. West. (LBL-13392, SAC-47).

48. Effects of Sample Size on the Stress Permeability Relationship for Natural Fractures by J.E. Gale and K.G. Raven. (LBL-11865, SAC-48).

49. Progress with Hydrogeological Characterization of the Stripa Site by J.E. Gale, A. Rouleau, P.A. Witherspoon and C.R. Wilson. (LBL-14878, SAC-49).

50. Extensometer Performance During Heater Experiments at Stripa by A.O. DuBois, M. Hood, E.P. Binnall and L. Andersson. (LBL-13531, SAC-50).

51. Seismic Velocities and Attenuation in a Heated Underground Granitic Repository by B.N.P. Paulsson (LBL-16346 1/2, SAC-51).

TABLE OF CONTENTS

LIST OF FIGURES

LIST OF TABLES

ABSTRACT

Thirty-five rod-type extensometers, each with four anchors, were installed in vertical and horizontal boreholes surrounding three groups of electrical heaters. These extensometers were part of instrumentation for three experiments investigating the thermomechanical behavior of a granitic rock mass. The site was a series of entries which had been extended, at the 340 meter level, from an inactive iron mine at Stripa, Sweden.

The extensometers were active and continuously monitored for approximately two years, during which time rod temperatures as high as 160°C were encountered. The mechanical and electrical behavior of various elements of these instruments have been examined and their reliability assessed. Laboratory tests on simulated extensometer installations have identified sources of the stick-slip behavior observed during the early weeks of the experiments.

1. INTRODUCTION

The thermomechanical response of a granitic rock mass subjected to thermal loading has been studied at Stripa, Sweden, as part of the cooperative Swedish-American Research Program described by Witherspoon and Degerman (1978). Electrically heated canisters simulated canisters containing high-level radioactive waste materials. These canisters were emplaced 340 meters below the surface in boreholes drilled into the floor and walls of horizontal entries (Kurfurst et al., 1978).

The heaters and the rock instrumentation were installed in three experimental areas (Figs. 1 and 2) to simulate a variety of borehole geometries and heat loads. The locations of all extensometer anchors and rod temperature sensors are shown schematically in Figs. 3a through 3e.

These experiments required the measurement of 750 channels of data. The parameters monitored over approximately two years of rock heating and cooldown were: heater input power; heater, rock, and instrument temperatures; rock displacement; and change in rock stress. All sensors had their output recorded by parallel systems of data loggers onto paper tape and by a central computerized data acquisition system (McEvoy, 1979). This same data acquisition system (DAS) was used for both pre-experiment and post-experiment calibration of the instruments. The constants determined by the pre-experiment field calibration procedures and others determined by laboratory tests were used by the computer for on-site conversion of voltage data from the sensors into engineering units. Subsequently, as a result of the post-experiment recalibration and additional tests, the calibration constants and engineering conversion algorithms were modified and the

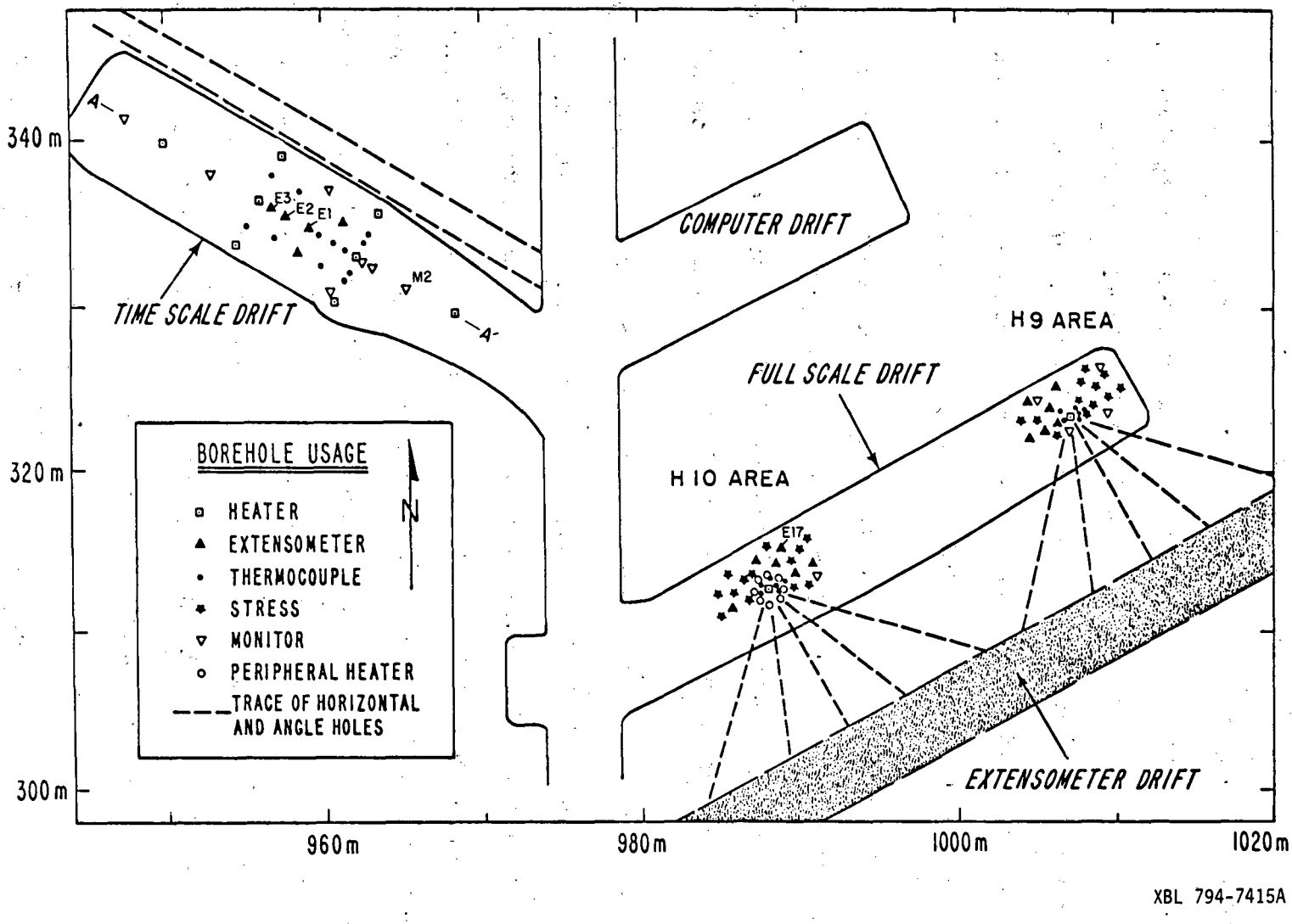

Fig. 1. Plan view of Stripa experimental area.

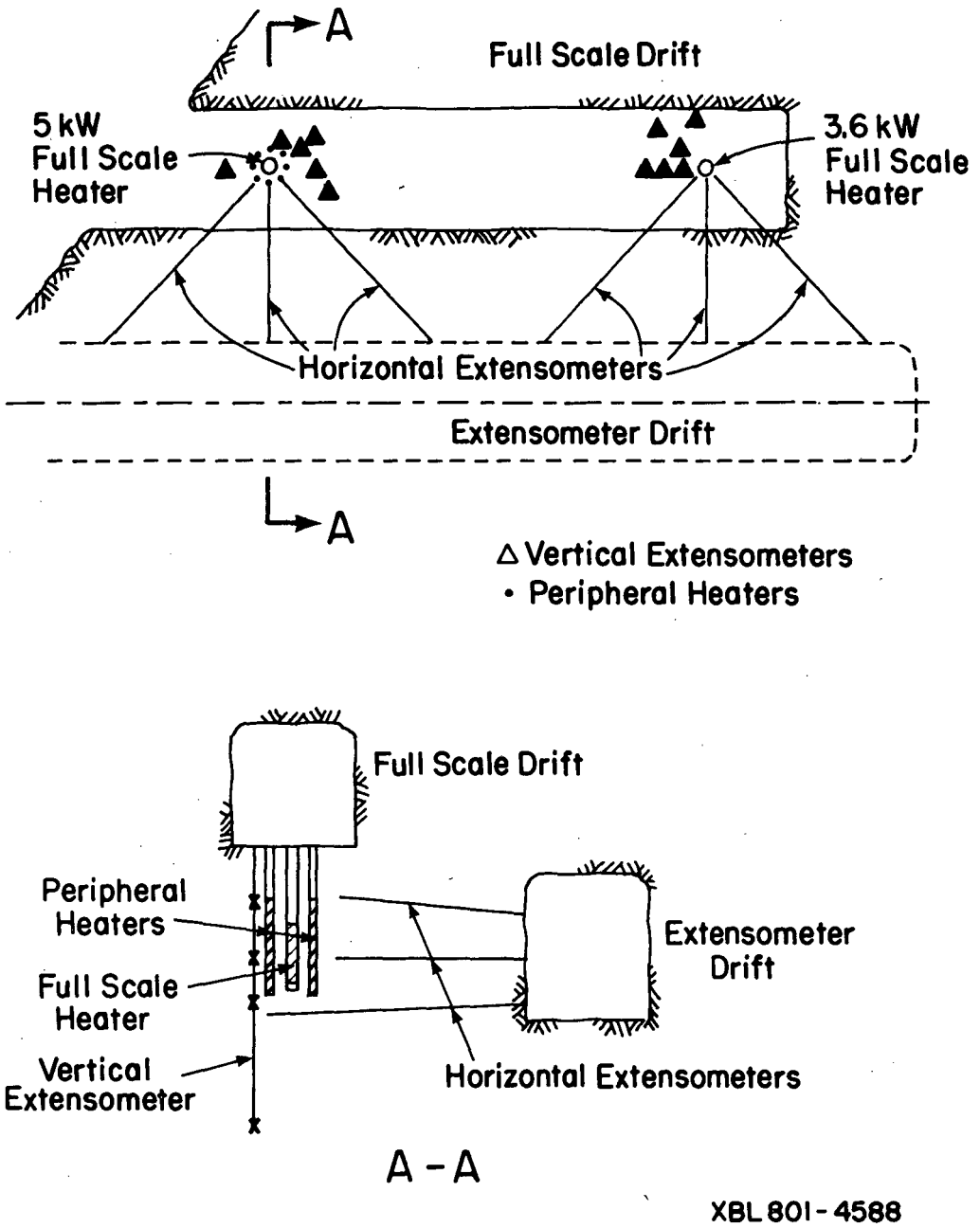

Fig. 2. Diagram of full-scale experiment boreholes.

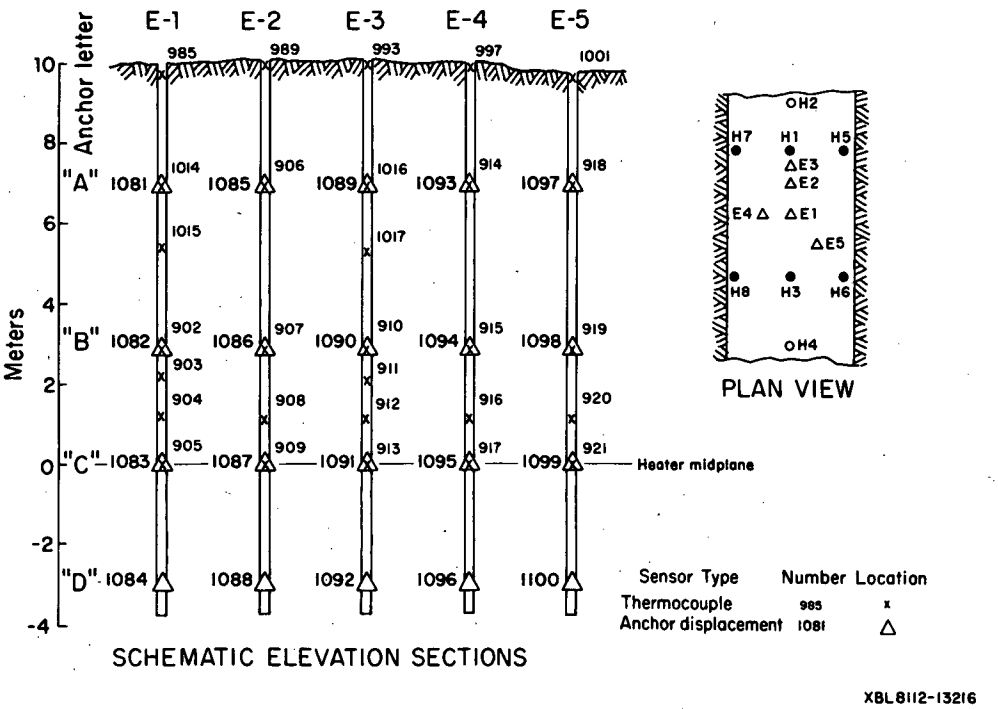

Fig. 3a. Location of anchors and thermocouples for vertical extensometers in the time scale experiment.

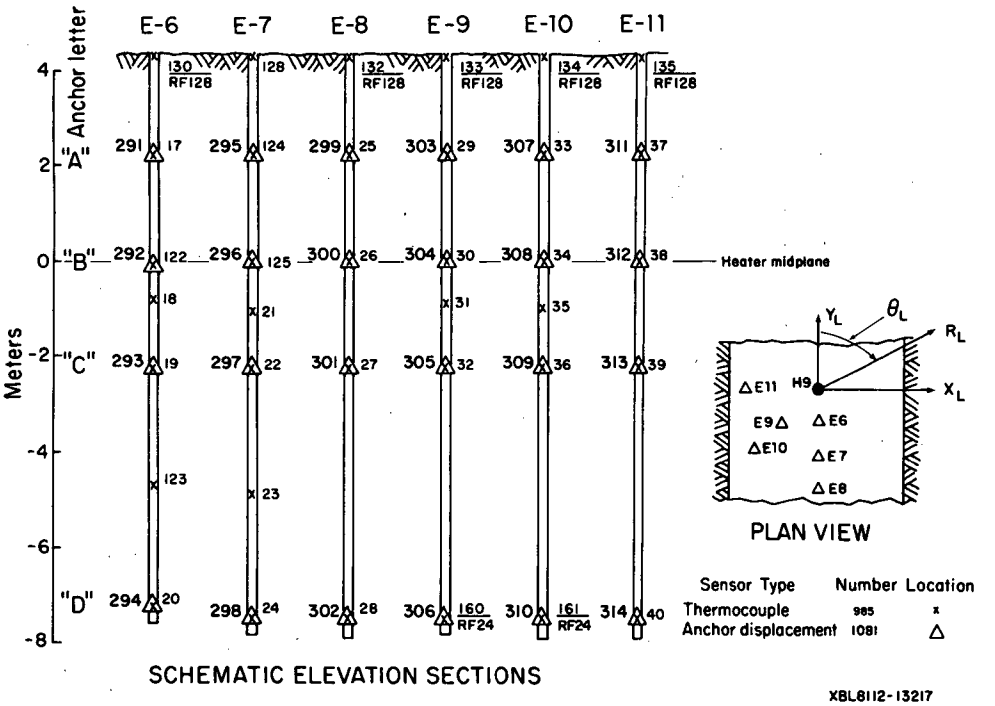

Fig. 3b. Location of anchors and thermocouples for vertical extensometers in the H9 experiment.

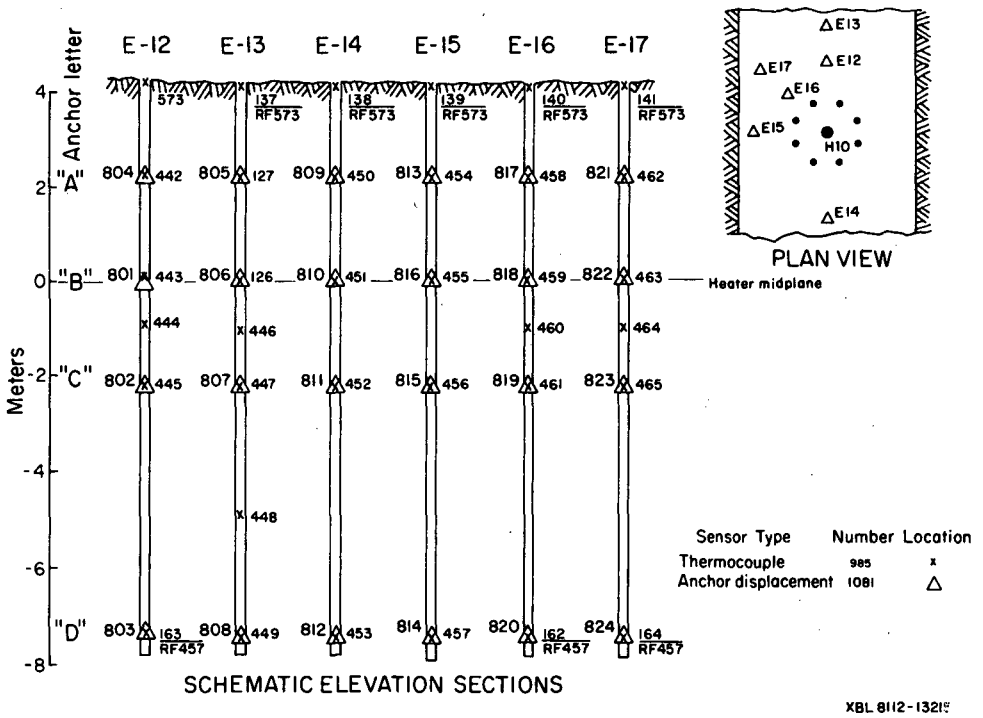

Fig. 3c. Location of anchors and thermocouples for vertical extensometers in the H10 experiment.

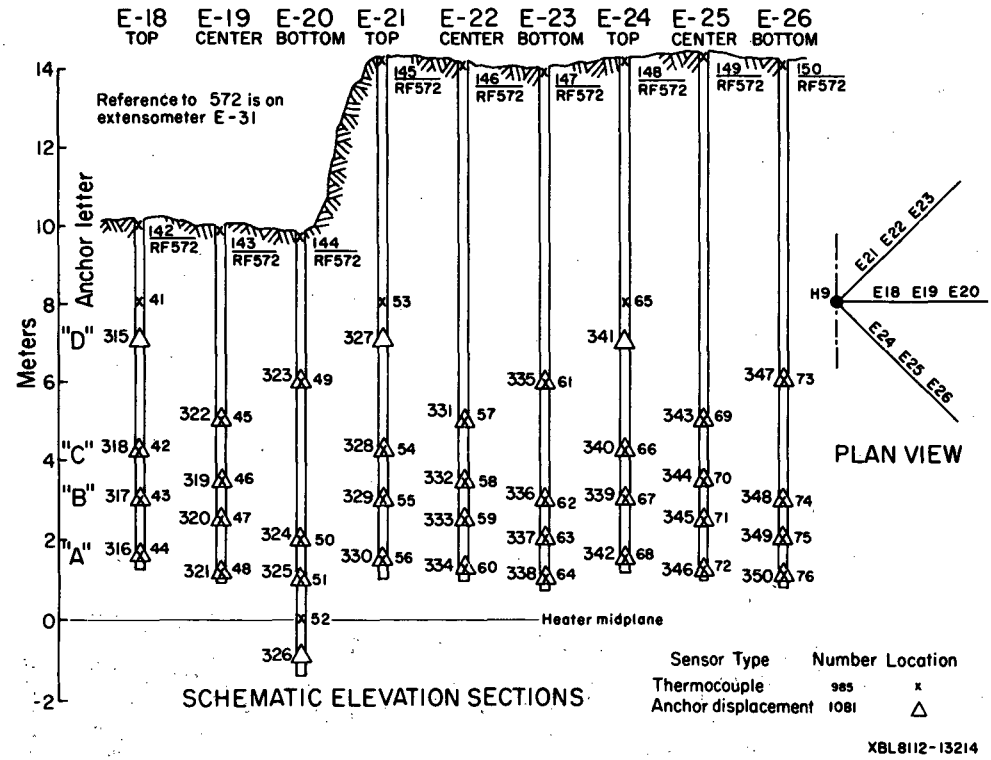

Fig. 3d. Location of anchors and thermocouples for horizontal extensometers in the H9 experiment.

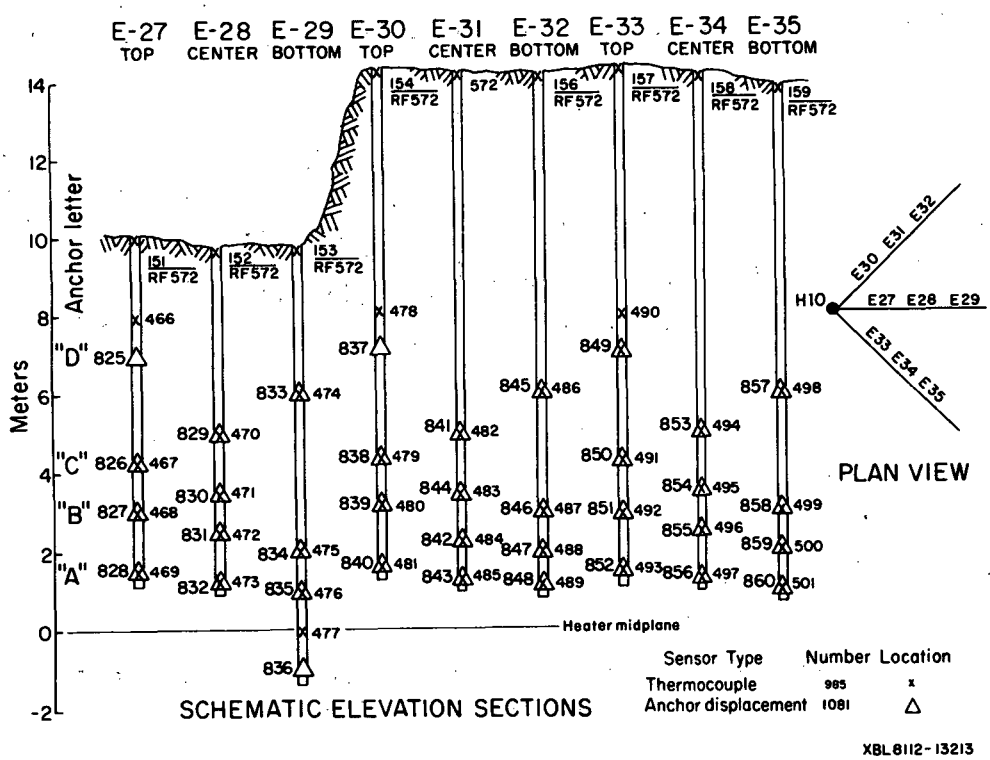

Fig. 3e. Location of anchors and thermocouples for horizontal extensometers in the H10 experiment.

voltage data reprocessed to yield a final record of engineering values (Chan et al., 1980). Figure 4 is a block diagram that summarizes the processing steps. A plot of the responses of each sensor (time-averaged engineering unit versus time) is available on microfiche in Appendix D of the Chan report. The time-averaging procedure cited in Fig. 4 is also described in that report.

This report will describe the operating experience and post-experiment calibrations of the 35 Stripa extensometers, as well as laboratory tests performed to better understand their frictional characteristics. Installation and pre-experiment calibrations of the extensometers were described in Schrauf et al. (1979). An interim report on extensometer operating problems was included in Binnall et al. (1979). For reports on other Stripa instruments, see Table 1.

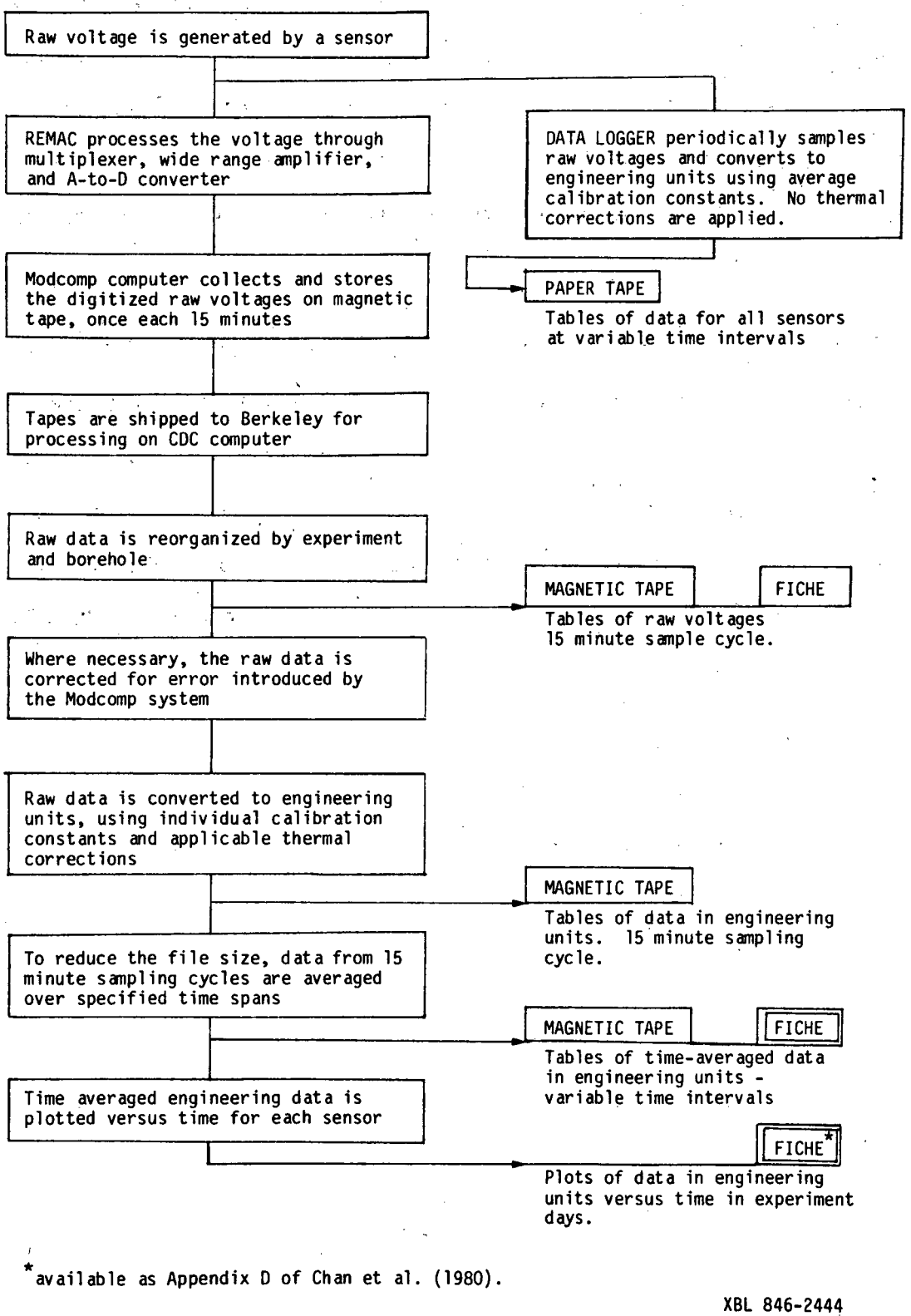

Fig. 4. Block diagram of extensometer data acquisition and processing.

Table 1. Guide to reports on heater experiment instrumentation.

Topic	Installation Report	Performance Report
Heaters	Burleigh et al. (1979; SAC-13)	No Report
Thermocouples	Schrauf et al. (1979, SAC-25)	Binnall and McEvoy (1981; in preparation)
Extensometers	Schrauf et al. (1979, SAC-25)	This Report
VWS and USBM gauges	Schrauf et al. (1979, SAC-25)	Lingle et al. (1984; in preparation)
Dewatering system	Schrauf et al. (1979, SAC-25)	Nelson et al. (1981; SAC-35)
Data acquisition	McEvoy (1979; SAC-14)	Chan et al. (1980; SAC-29)

2. DESCRIPTION OF EXTENSOMETERS

The four-anchor extensometer used at Stripa was a customized version of a model 4CSLT-R instrument manufactured by Terrametrics Inc., Golden, Colorado. One spring-tensioned Superinvar rod (6.35 mm diam and up to 13 m long) connected each of the four downhole anchor points to one of four displacement sensors (25 mm range) located at the borehole collar. A simplified schematic of a two-anchor installation is shown in Fig. 5. Note that a waterproof flexible conduit isolates the rods from the borehole environment. The rods enter the collar stabilizer tube via a Nylon fleet-angle bushing. The rods take a slight radial offset as they pass from that bushing to their individual spring-tensioned guide tubes. Plastic bushings in the head assembly support each guide tube.

The rod displacement sensor, a direct-current displacement transducer (DCDT), is model 243-0011 manufactured by Trans-Tek Inc. of Ellington, Connecticut. The transducer is an integrated package consisting of a precision linear variable differential transformer (LVDT), a solid-state oscillator, and an AC- to DC-rectification circuit. The core, when displaced axially within the coil assembly, produces a DC output voltage change proportional to the displacement. All DCDT sensors in the time-scaled experiment were powered from a single remote, regulated DC power supply. The DCDT sensors in the two full-scale experiments were powered from a second supply.

After an extensometer was inserted into its borehole, grout was injected into the annular space between the conduit and the borehole

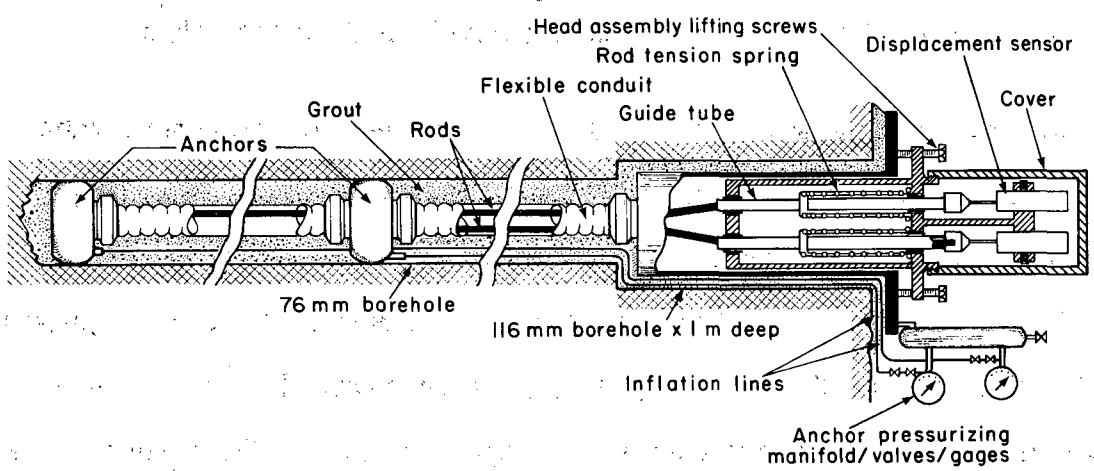

Fig. 5. Mechanical schematic of an extensometer. Simplified version shown with only two anchors.

wall. This grout aided in securing the anchors and prevented the circulation of ground water within the borehole. If the borehole were left as an open conduit, any convection or ground-water flow might disturb the thermal field along the borehole. While the grout was still fluid, the anchors were hydraulically pressurized to secure them in the borehole (Fig. 6). The hydraulic pressure for each anchor was monitored and adjusted throughout the experiment to compensate for pressure changes resulting from thermal expansion of the pressurizing fluid.

Four to seven thermocouples were taped to the longest rod in each borehole to sense the rod temperature profile. (There were 158 thermocouples in all.) All four rods in a borehole were assumed to be at the same temperature at any given depth so that the temperature profile, and hence the thermal expansion, applied to each. The calculated expansion was applied as a correction to the rod displacement sensor output. To minimize this thermal expansion correction term, Superinvar alloy (64% Fe, 31% Ni, 5% Co) was selected.

The algorithm for conversion of the output voltage of an extensometer sensor into engineering units for rock displacement is described by Chan et al. (1980). Both the Chan report and this one use the rock mechanics convention in which contraction is assumed to be a positive displacement. A more detailed description of the extensometers and their pre-experiment testing, installation, and calibration appears in Schrauf et al. (1979).

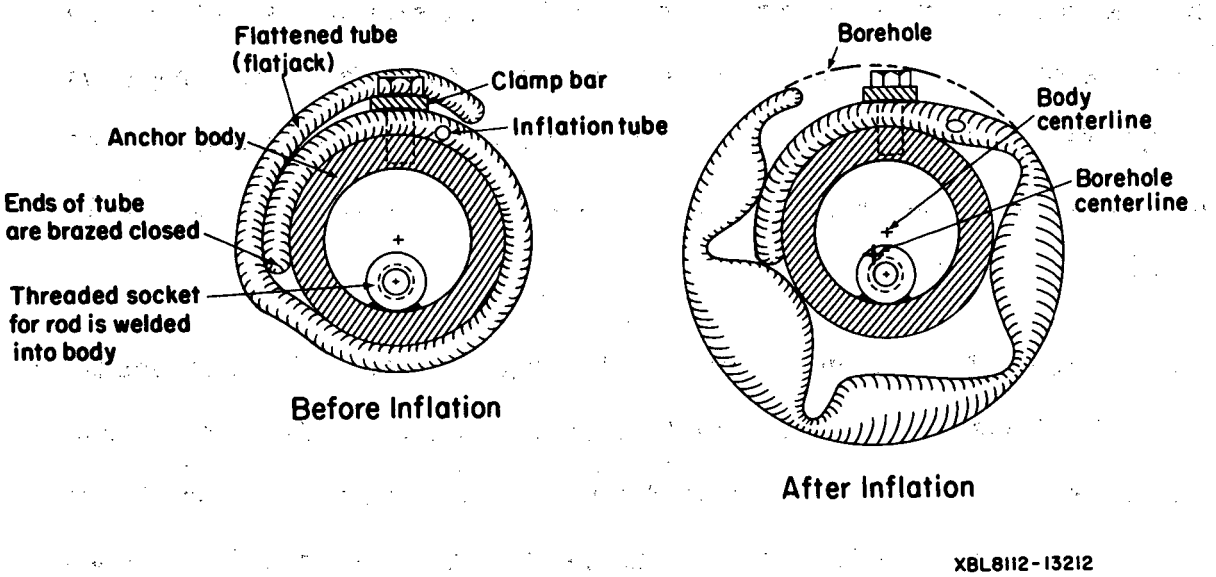

Fig. 6. Cross section through an inflatable anchor.

3. OPERATIONAL HISTORY

3.1 General

Thirty-five extensometers were installed and calibrated in May and June 1978. The time-scaled experiment was started when its eight heaters were energized on June 1, 1978; five vertical extensometers were used (Fig. 3a). The full-scale heater "H1O" was energized on July 3, 1978, and the eight peripheral heaters surrounding it were energized on January 23, 1979. This 5-kW heater and its eight one-kW peripheral heaters were surrounded by six vertical and nine horizontal extensometers (Figs. 3c and 3e). The "H-9" full-scale heater (3.6 kW), energized on August 24, 1978, also was surrounded by six vertical and nine horizontal extensometers (Figs. 3b and 3d). Each full-scale heater array was energized for approximately 12 months, and the rock instrumentation continued to be monitored for an additional six months of cooldown. Final recalibrations and circuit verifications were performed before shutdown of the data acquisition system in June, 1980.

All 140 of the DCDT sensors (4 anchors x 35 boreholes) operated over the entire experiment. One sensor changed its calibration factor by approximately 12%; the others changed by an average of approximately 1%. All but one of the 158 thermocouples sensors, which were mounted on the Superinvar rods, also performed well throughout the experiment.

3.2 Range of DCDT Response

The anchor-to-collar displacements, after correction for thermal expansion of the rods, ranged from a maximum of 0.6 mm of extension

(on a horizontal extensometer) to 3.1 mm of contraction (on a vertical extensometer). Because of variations in the transducer starting output voltages, the range of DCDT sensor outputs (Fig. 7) varied between -1.5 V and +0.25 V. Over this range of voltages, the least count of the multi-range amplifier and D-A converter in the Modcomp computer did not exceed 1.25 mV--equivalent to about 3 μm of displacement. The noise level in the computer data was greater for output voltages near zero volts because the wide-range amplifier, which automatically ranged to higher amplification for smaller signals, was less able to reject common-mode noise in the highest amplification ranges.

3.3 Thermal Environment

All but one of the Chromel-Alumel thermocouples survived, providing an essentially continuous rod-temperature record. The one exception was damaged during installation. Table 2 lists the maximum temperature measured in each extensometer borehole. Figure 8 shows the temperature history for the hottest anchor (E31A). Plots of temperature versus time are provided for all extensometer thermocouples in Appendix D of Chan et al. (1980). Figure 9 shows the temperature profile along extensometer E-29 (which passed directly under the H-10 heater) just before heater turn-off. This profile, when combined with the coefficient of thermal expansion data for Superinvar (Schrauf et al., 1979), allows one to calculate the thermal expansion of each rod in that borehole (Table 3). The rods of E29 passed through some of the hottest parts of the rock.

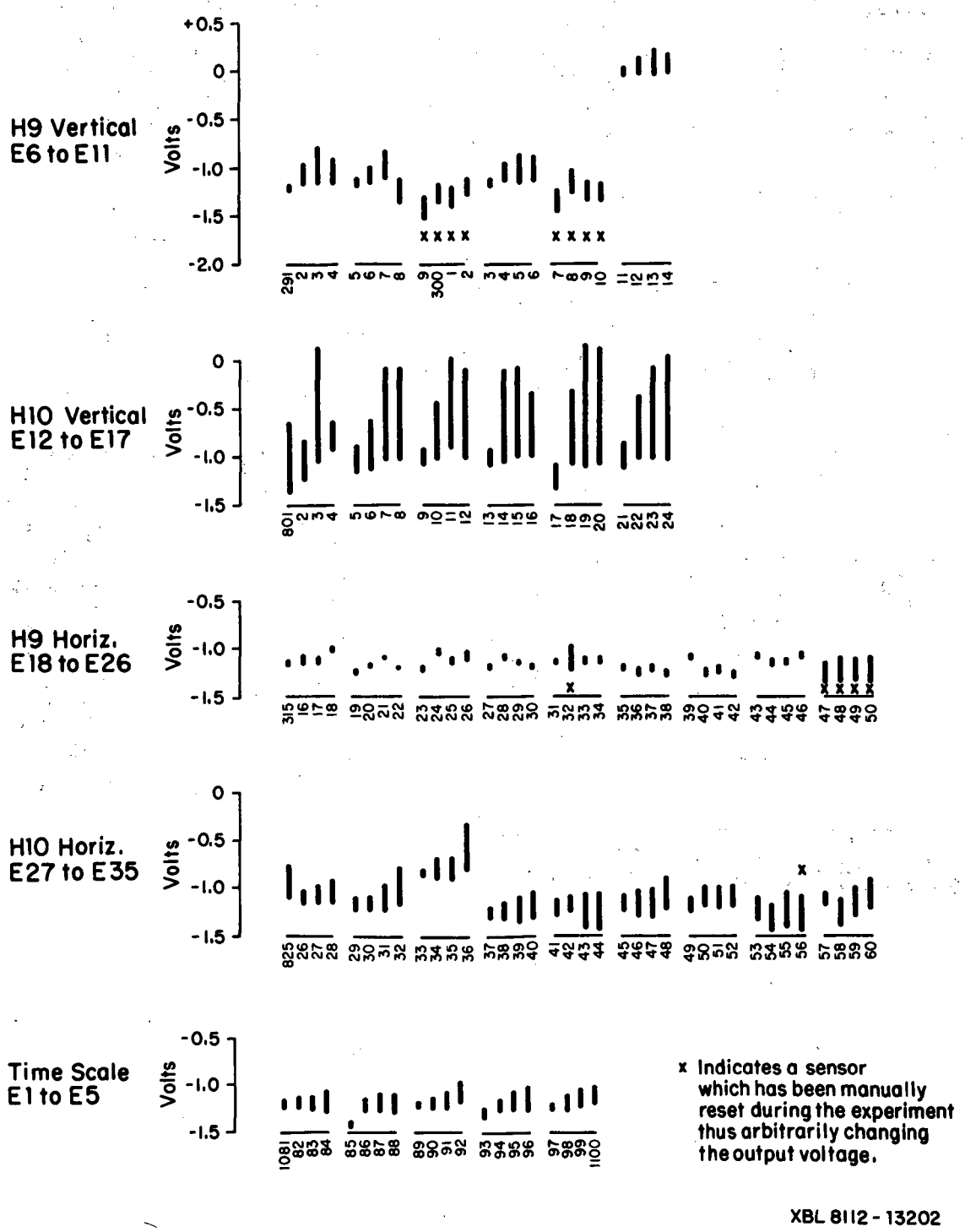

Fig. 7. Voltage output range for each displacement sensor.

Table 2. Maximum temperature measured in each extensometer borehole.

Experiment	Vertical Borehole	Maximum Temperature, °C	Horizontal Borehole	Maximum Temperature, °C
Time-Scaled	E1	25.0	--	--
	E2	28.7	--	--
	E3	35.6	--	--
	E4	25.0	--	--
	E5	27.5	--	--
H9	E6	69.0	E18	34.8
	E7	40.0	E19	55.8
	E8	29.4	E20	50.1
	E9	51.5	E21	35.2
	E10	33.9	E22	56.5
	E11	38.9	E23	38.9
	--	--	E24	35.6
	--	--	E25	58.8
	--	--	E26	40.3
H10	E12	101.0	E27	89.4
	E13	64.1[a]	E28	154.8
	E14	78.6	E29	146.9
	E15	98.2	E30	83.9
	E16	123.3[b]	E31	159.2
	E17	77.3	E32	110.5
	--	--	E33	87.9
	--	--	E34	158.8
	--	--	E35	110.5

[a] Temperature limited by water in conduit.
[b] Before water leaked into conduit.

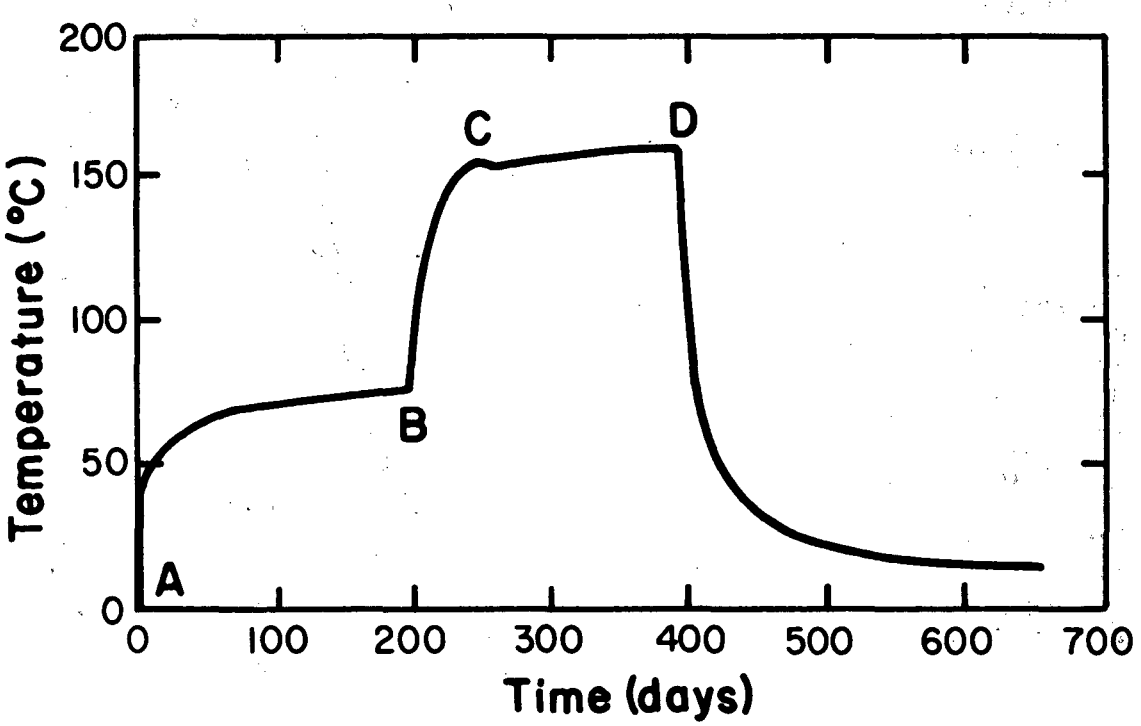

A 5 kW heater on
B Peripheral heaters on at 1.0 kW
C Peripheral heaters reduced to 0.85 kW
D All heat off

XBL 8112-13203

Fig. 8. Temperature history of warmest point on a Stripa extensometer. Thermocouple sensor No. 843 at the depth of the deepest anchor on vertical extensometer E31.

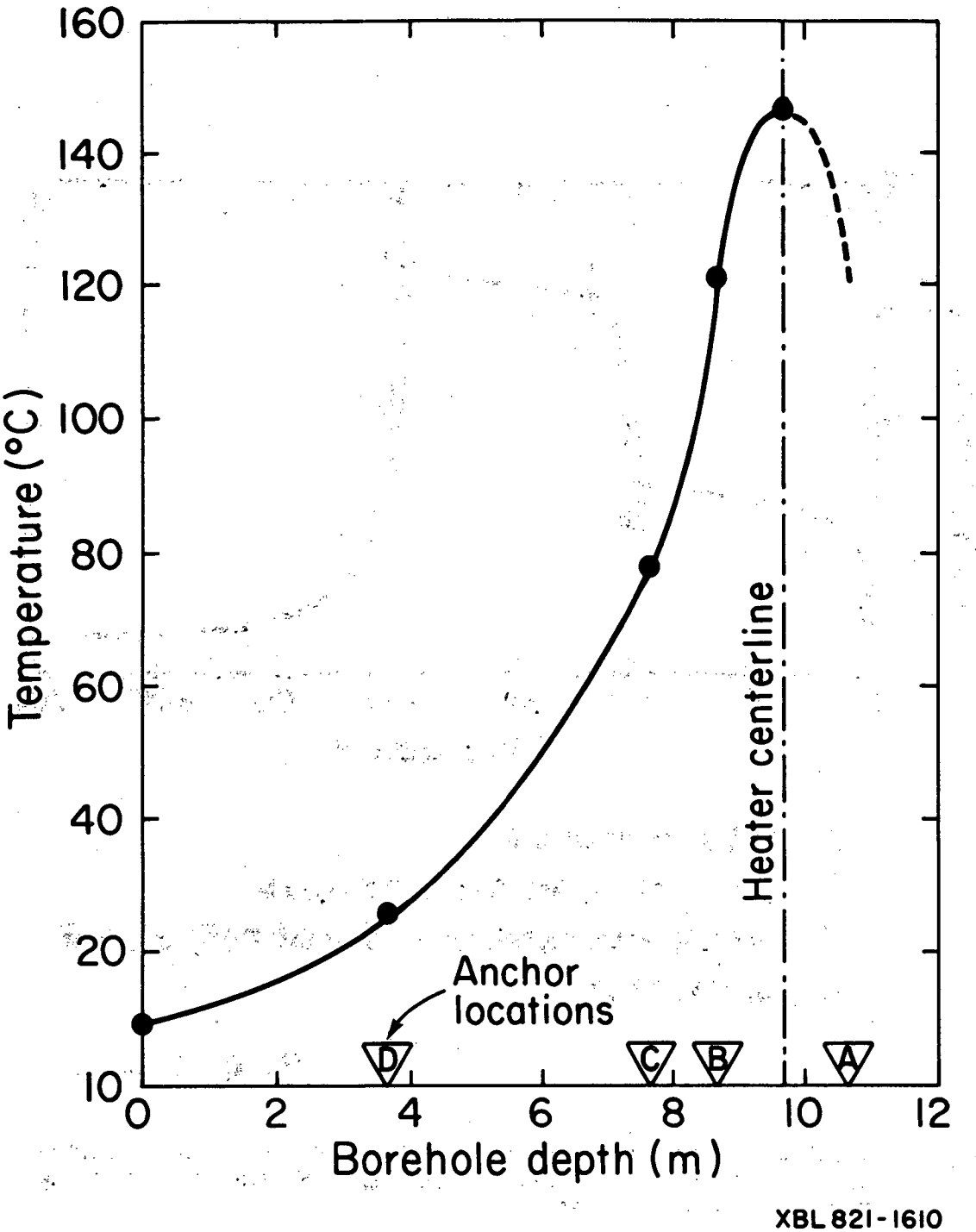

Fig. 9. Temperature profile along horizontal extensometer E29. Experiment day 394. A cubic spline curve is fit to the five thermocouple temperature measurements. The temperature profile is assumed to be symmetrical about the heater center line.

Table 3 Thermal expansion data for extensometer E29.

(a) Thermal expansion for each rod of E29 and its relationship to the displacements measured between the collar and the anchors on experiment day 394--just before heater turn-off.

1	2	3	4	5	6
Rod/Anchor Number	Rod Length (m)	Gross Displacement (mm)	Thermal Expansion (mm)	Correction (%)	Net Displacement (mm)
A	10.64	-1.040	-0.363	35	-1.403
B	8.64	-0.139	-0.093	67	-0.232
C	7.63	+0.017	-0.029	171	-0.012
D	3.63	-0.004	-0.001	25	-0.005

(b) The displacements between adjacent anchors, compared on the basis of gross and net displacements.

7	8	9	10	11
Rod Span	Gross Displacement (mm)	Thermal Expansion (mm)	Correction (%)	Net Displacement (mm)
A-B	-0.901	-0.270	30	-1.171
B-C	-0.156	-0.064	41	-0.220
C-D	+0.021	+0.007	133	-0.028

Notes: Column 5 = 100 x Column 4 ÷ Column 3
Column 10 = 100 x Column 9 ÷ Column 8
Negative displacement represents extension.

The temperature profile along a typical vertical extensometer is shown in Fig. 10. Two of the vertical extensometers had temperature profiles which were unusual in that: (a) near the heater midplane, the profile was flatter than expected, and (b) the profile was not symmetrical about the heater centerline (Figs. 11 and 12). We interpret these profiles to be clear evidence that, in these cases, water had entered the "waterproof" conduit. Because of the temperature profile, the water below the heater midplane increases in density with increasing depth so that convection currents are not generated. Above the midplane, the density gradient is reversed; the convection currents thus generated transport heat away from the warmer region near the midplane and carry that heat to the cooler region above the midplane.

The pattern is somewhat different in the case of E16 (Fig. 12). Our interpretation is that mixing occurs for some depth below the midplane because the temperatures there are high enough to create steam bubbles. Those bubbles modify what would otherwise be a positive density gradient, and convection occurs to the depth at which boiling occurs.

In addition, the distorted profile of E13 existed at all times, but that of E16 was established suddenly on experiment day 240. We conclude that the waterproof covering for E13 was damaged during installation, whereas E16 was dry until the temperature reached 120°C and caused a seal failure. The conduit adapter fitting, which couples the downhole protective conduit to each anchor, uses a molded plastic ring or gasket to make a

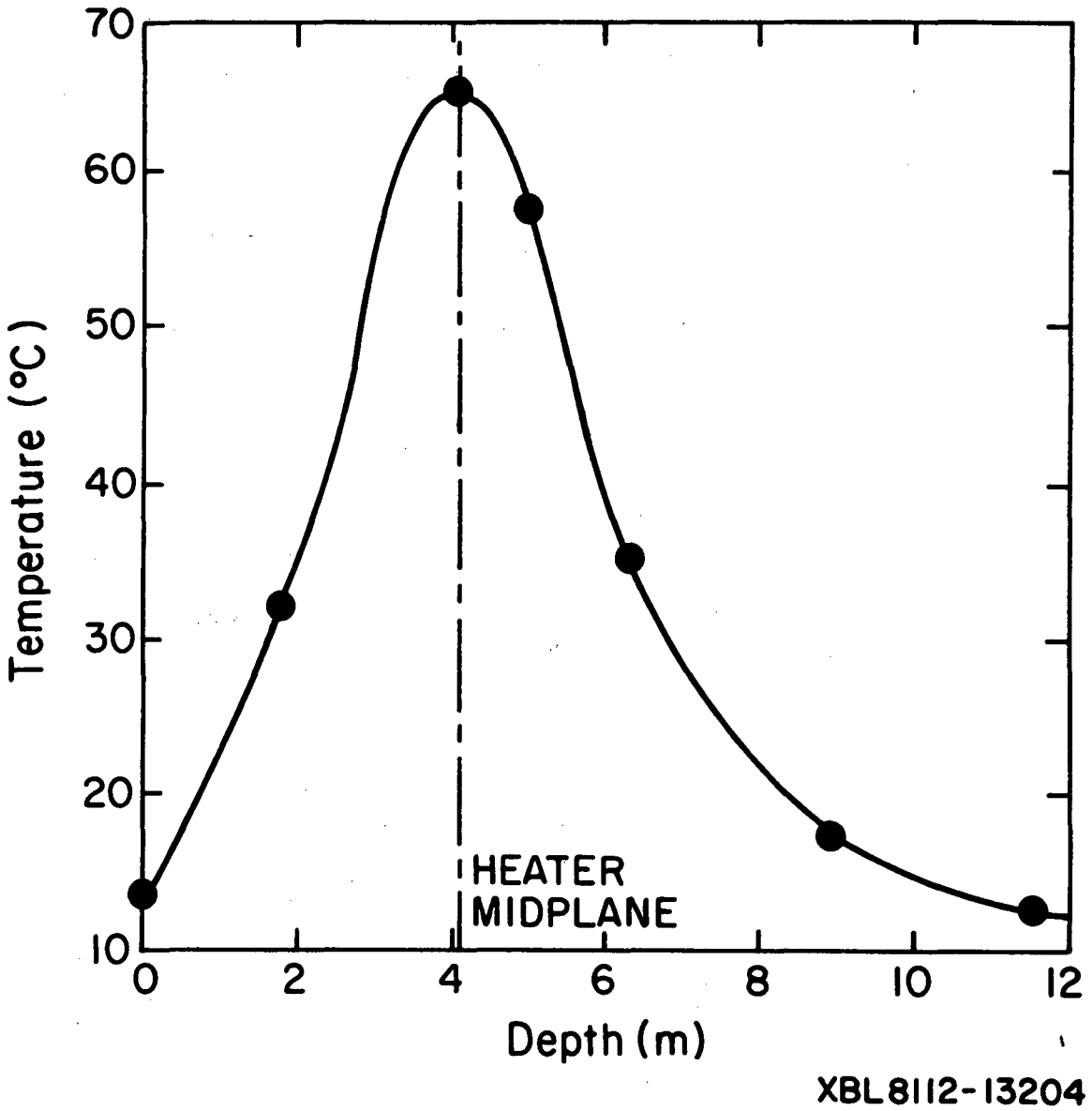

Fig. 10. Temperature profile along extensometer E6. Experiment day 150.

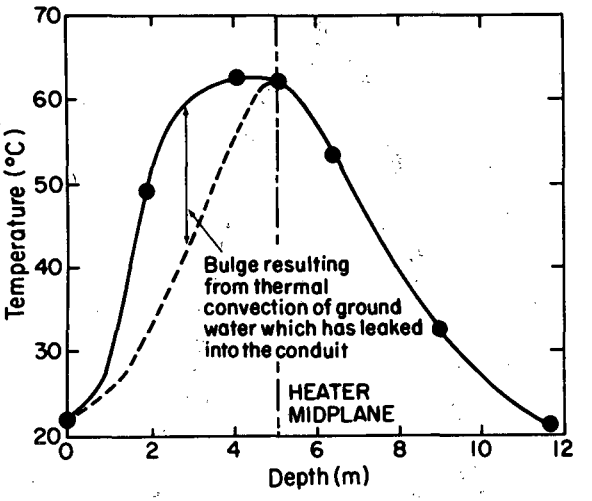

Fig. 11. Temperature profile along extensometer E-13. Experiment day 394.

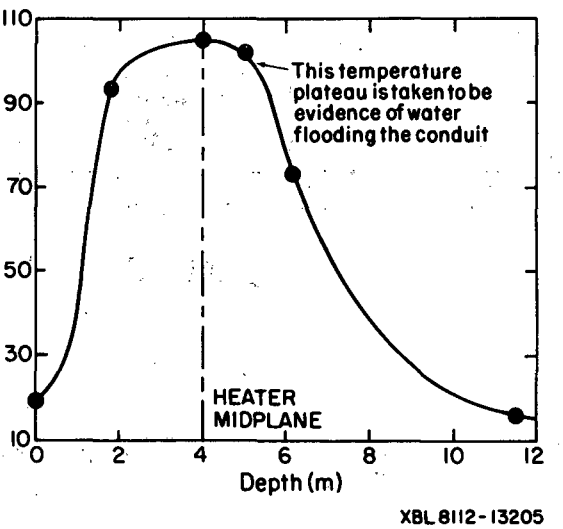

Fig. 12. Temperature profile along extensometer E-16. Experiment day 245.

waterproof seal. We believe this ring relaxed its sealing force when its temperature reached 120°C and that this relaxation precipitated the seal failure. In a laboratory test, the ring distorted when placed in boiling water. When the flame from a match was brought within one-half inch another of these plastic rings, the ring melted and changed from a milky to a water-clear appearance. We believe it was polyethelene, which is unsuitable for an elevated temperature environment.

No vertical extensometer besides E16 experienced temperatures above 101°C, and because they inclined downward toward their collars none of the horizontal extensometer holes flooded. However, horizontal extensometers E26, E27, E28, E29, E32, and E34 had water leakage that flowed down the inclined conduit and accumulated in the protective can covering the sensors. The interiors of some other covers felt damp when touched. After the leakage was discovered, a weep hole was added to the covers of all horizontal extensometers to provide continuous drainage.

The rod temperature, because of its effect on Young's modulus, may have had an additional impact on the extensometer records. Invar alloys are unusual in that, at temperatures near ambient, they have a positive thermoelastic coefficient, i.e., Young's modulus rises with test temperature. According to the International Nickel Company (1962) a 31% nickel alloy will have a thermoelastic coefficient of $+41 \times 10^{-5}/°C$. If one assumes that this value is valid for Superinvar and that it is constant over the range of temperatures measured in the Stripa extensometer holes, the maximum effect this coefficient might have had can be calculated. For rod E29A, which experienced the largest (50°C) increase in average

temperature, the maximum change in rod length, resulting from this modulus change, would have been 22 μm for this 9.64 m rod under an axial load of approximately 445 Newtons.

3.4 Anchor Inflation

During extensometer installation, each flatjack anchor was inflated to 1800 psi. The pressurized anchor and its pressure monitoring gauge were then isolated from the inflation manifold by a pair of manual valves. As the heater test progressed, the thermal expansion of the hydraulic inflation fluid caused the anchor pressure to increase. After the heaters were turned off, the temperatures and pressures decreased. Throughout the experiment, the inflation pressure in each anchor was periodically monitored and readjusted to maintain the pressure between 1,500 and 2,500 psi. At the beginning of the H-10 experiment, when the nearest anchor temperatures were increasing rapidly, the pressure in one anchor (E28A) increased by 1,000 psi in 24 hours. Another anchor (E6B) was inadvertently allowed to reach 3,400 psi. This excessive pressure did not rupture the flatjack, and this anchor appeared to perform well for the remainder of the experiment. A hydraulic system incorporating a gas-over-oil accumulator would have done much to mitigate the pressure excursions.

Because of hydraulic leaks that developed in some anchors, or in their connecting plumbing, lower pressures were sometimes observed. Two anchors (E22-D and E27-D) showed evidence of anchor fluid leakage from the time of installation, and three anchors (E19-C, E21-D, and E29-C) failed completely during the initial pressurization. Eleven of the 140

anchors had completely lost pressurization by the end of the experiment, when the pressures of all anchors were measured; these pressures are listed in Table 4. Temperature did not seem to be the critical parameter in causing anchor pressure loss. The two hottest anchors (159°C) performed well throughout the experiment.

None of the sensors associated with the anchors that lost pressurization showed an identifiable change in their output as a result. These anchors were apparently secured adequately by the combined effects of the grout and the initial plastic deformation of the flatjacks. Post-experiment rod-pull tests (described below) were performed on most of the extensometers. These pull tests also failed to show evidence of anchor slip. A bench test, however, showed that an ungrouted anchor, inflated to 2,000 psi within a 3-inch steel pipe, could be caused to move axially under as little as 75 pounds force.

3.5 Rod Friction

Within the first 100 experiment days, it became obvious that many sensors were responding in a stepwise fashion (Hood, 1979). One explanation was that the rock was experiencing a stick-slip behavior related to closure of fractures. In February 1979, an ultrasonic detector was placed in an open borehole to correlate the timing of any acoustic emission (as an indication of rock slippage) with the stepwise output of an extensometer but, during ten days of observation, no such correlation was observed.

With this natural cause eliminated, it became important to find the actual source of this stepwise behavior, as the data being collected could otherwise be called into question.

Table 4. Anchor pressures (psi) on April 25, 1980.[a]

Time-Scaled Experiment

Vertical Boreholes

Rod	E1	E2	E3	E4	E5
A	1750	1900	1800	1700	1600
B	1700	1600	1100	1330	1600
C	1600	1750	1720	0	1500
D	1600	1750	1750	1800	1700

H-9 Experiment

Vertical Boreholes

Rod	E6	E7	E8	E9	E10	E11
A	800	1650	1650	1390	1560	1720
B	1520	1550	1110	1210	1600	1510
C	1510	1300	1030	1590	1610	1660
D	1520	610	1600	1600	1420	1530

Horizontal Boreholes

Rod	E18	E19	E20	E21	E22	E23	E24	E25	E26
D	880	200	1400	0	1160	1560	1510	1400	1525
C	1100	0	1580	1380	1250	1350	1480	1530	1410
B	1430	1200	1280	1620	1210	1100	1160	1550	500
A	1450	0	1700	1150	1490	1280	1580	0	1550

H-10 Experiment

Vertical Boreholes

Rod	E12	E13	E14	E15	E16	E17
A	1390	1410	1420	1390	1300	1290
B	450	1190	1560	1520	0	1500
C	1500	820	1500	1520	1410	1150
D	1570	1550	1620	1550	0	1510

Horizontal Boreholes

Rod	E27	E28	E29	E30	E31	E32	E33	E34	E35
D	820	1250	1320	1310	1340	1510	1320	1600	1600
C	1320	1250	0	1500	1360	1510	1550	1520	1540
B	1350	1200	1150	1450	1250	1400	980	850	1550
A	0	0	1100	1480	1310	0	1600	1500	1550

[a] Anchors are listed in order of increasing distance from borehole collar.

Frictionally stored displacement within the instrument is believed to be the cause of the stepwise responses, the evidence is as follows. On February 15, vibrations from pounding in an open borehole (M 10) near the H-10 experiment correlated with the stepwise changes in sensor output from many nearby extensometers. On February 19, the rock face of the extensometer drift was pounded with a hammer near extensometers E27, E28, and E29. Their transducers immediately responded with a stepwise output. On February 20, the protective covers of extensometers E12, E13, E16, E29, E34, and E35 were rapped with the plastic handle of an 8-inch screwdriver. In each case, a stepwise response was observed.

To evaluate this behavior more directly, a previously undisturbed vertical extensometer head (E5) was vibrated by rapping the side of its protective steel cap with the plastic handle of an 8-inch screwdriver. Figure 13 shows the response of the four sensors on E5 when the head was given a series of raps spaced over a period of six minutes. The stepwise response ranged from -0.001 mm (on the shortest rod) to 0.081 mm (on the longest). The long-term response of the sensor connected to the deepest anchor of E5 is shown in Fig. 14. Other extensometers tested in this fashion behaved similarly, although, E15, showed no response. A possible explanation is that daily foot traffic nearby provided sufficient vibration to prevent the accumulation of frictionally stored rod displacement.

As a result of this evidence each extensometer head was vibrated by thumping three times daily (except weekends and holidays) with a plastic hammer. The frequency was reduced to once per week during the final portion of the experiment, when the rock temperature was nearly stable.

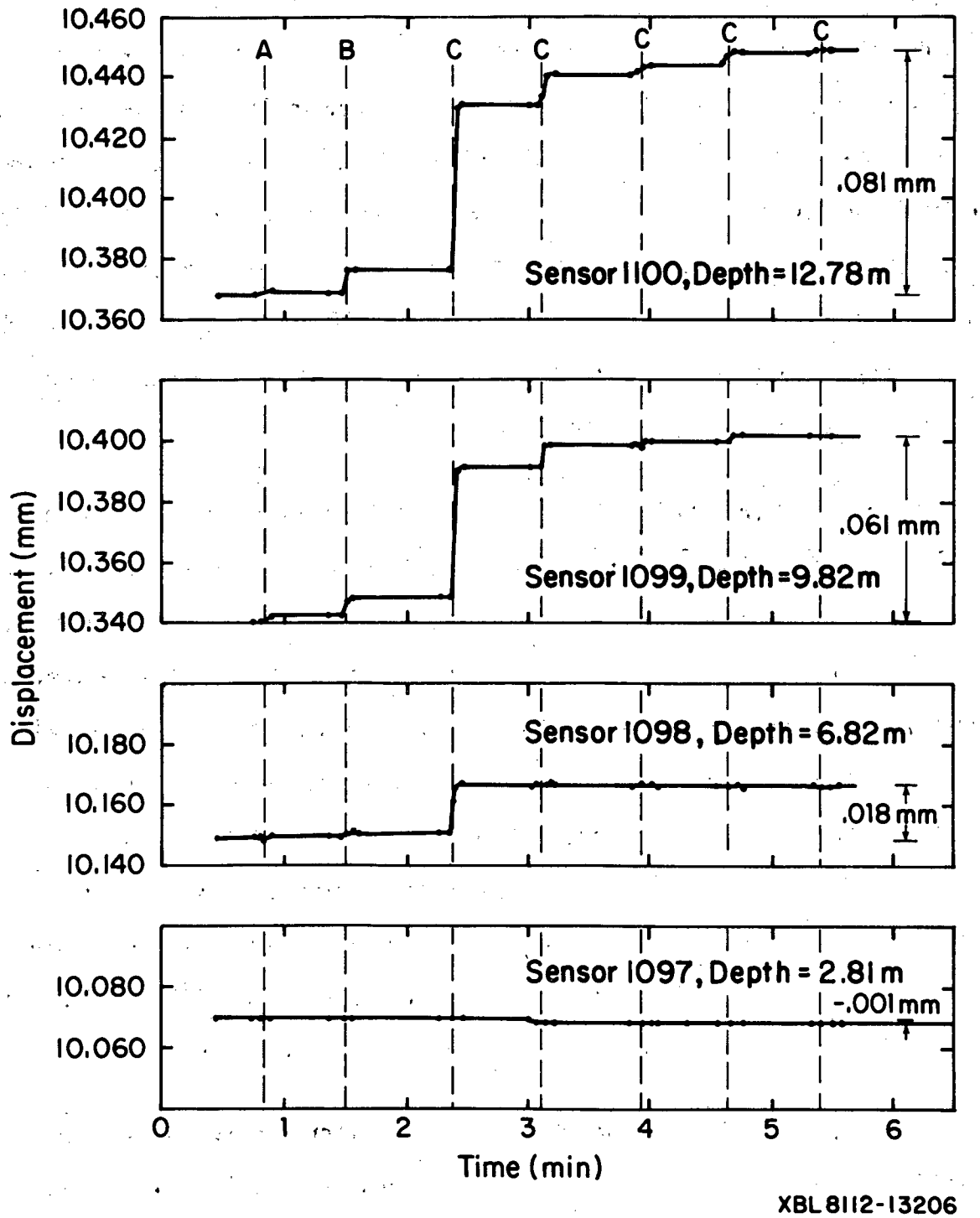

Fig. 13. Stick slip response of extensometer E-5.
A = one light tap (with plastic handle of screw driver)
B = three light taps
C = three firm taps

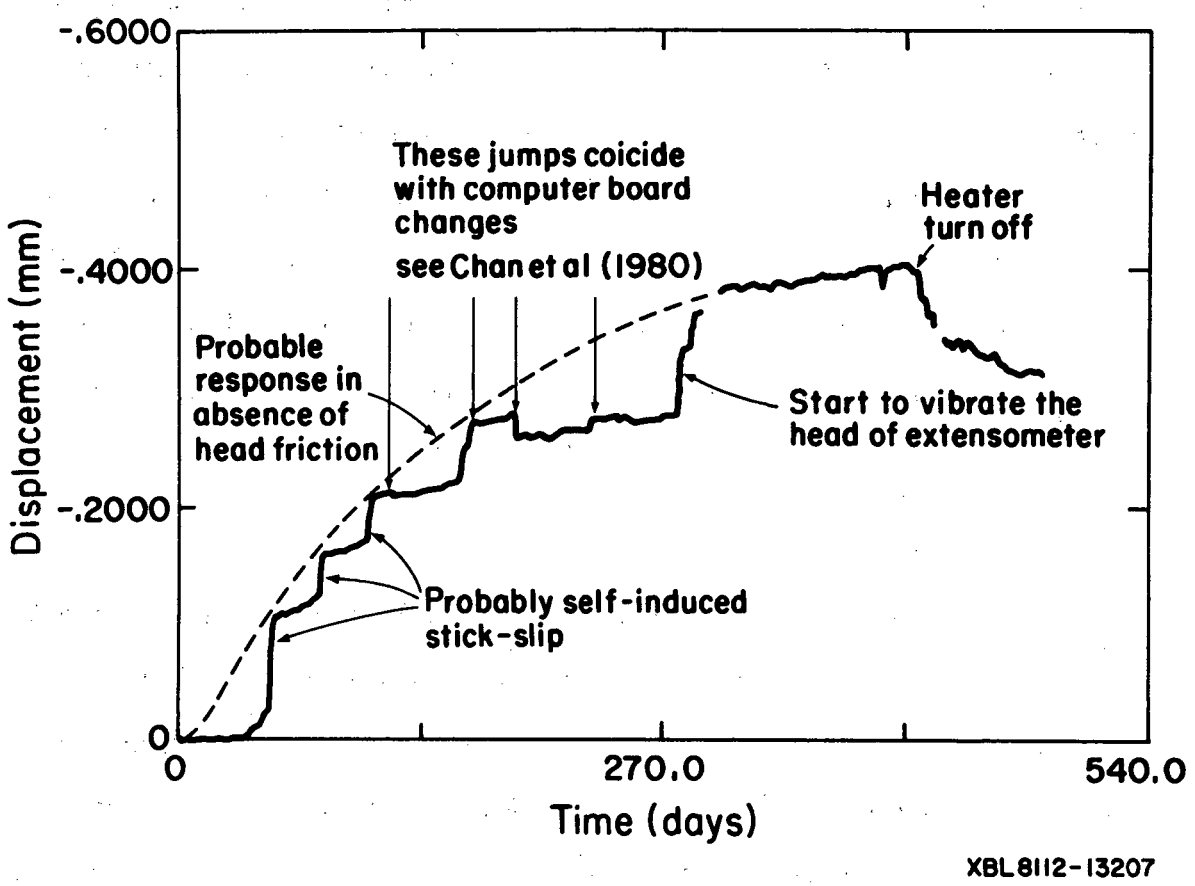

Fig. 14. Displacement record for extensometer E-5D.

Thumping was effective in reducing the amplitude of the stepwise response; however, one hazard of this procedure did appear. Some of the set screws that position a DCDT coil within the head assembly were later found to be loose. Some of these coils may have moved when vibration loosened their retaining set screws. The displacement records for E18-C and E22-C are believed to show evidence of this coil slippage problem in that their output continued to drift off in one direction at a time when little rock displacement was anticipated. Additional evidence of instrument friction is given in Section 5, describing laboratory tests.

3.6 DCDT Power Supply Voltage

One power supply provided input power to all time-scaled experiment extensometers, and a another supplied all full-scale (H9 and H10) experiment extensometers. Each was set for 10.565 V output before the initial extensometer calibration. This voltage level was checked and adjusted periodically for minor deviations; it was adjusted once (Jan. 31, 1979), when significant deviations were noted.

On the latter occasion the power supply for the time-scaled experiment was reset from 10.553 to 10.565 V and the full-scale power supply was reset from 10.527 to 10.565 V. During recalibration, it was demonstrated that this change in the DCDT excitation (from 10.527 to 10.565 V) would have caused a change of DCDT output of less than 5 mV, equivalent to about 10 μm displacement. Before the post-experiment recalibration, the power supplies were verified to be at their nominal 10.565 output voltage.

3.7 Electrical and Water Problems

As the experiment progressed, an increasing amount of noise was apparent in some extensometer signals. A particularly severe example occurred on Feb. 21, 1979, when sensor E29A indicated a large, rapid movement (Fig. 15). Upon removal of the protective cover on February 26, a large quantity of brown water poured out. Water from the granite formation was entering the flexible conduit surrounding the Superinvar rods and flowing to the lowest point in this horizontal extensometer--the head. The brown color of the water was undoubtedly evidence of rusting. The terminal strip and part of two sensors had been submerged. Heavy corrosion deposits covered the screws on the terminal strip, and many wires broke when moved. Every fourth terminal space (power-supply positive voltage) was completely filled by a heavy black deposit plated to the terminal.

The remaining 17 horizontal extensometers were then inspected. E26 was drenched in water and E34 was damp. The others were dry. All horizontal extensometer covers were drilled to provide weep holes. Three months later, water was dripping from E26 in the H-9 experiment and from E27, E28, E29, E32, and E34 of the H-10 experiment.

Even some of the extensometers that were nominally dry had enough condensation and corrosion in the terminal strip to create electrical noise problems. Several steps such as tightening screws and replacing connections improved the reliability of the signals; but the greatest improvement resulted from deleting the terminal strip entirely, soldering

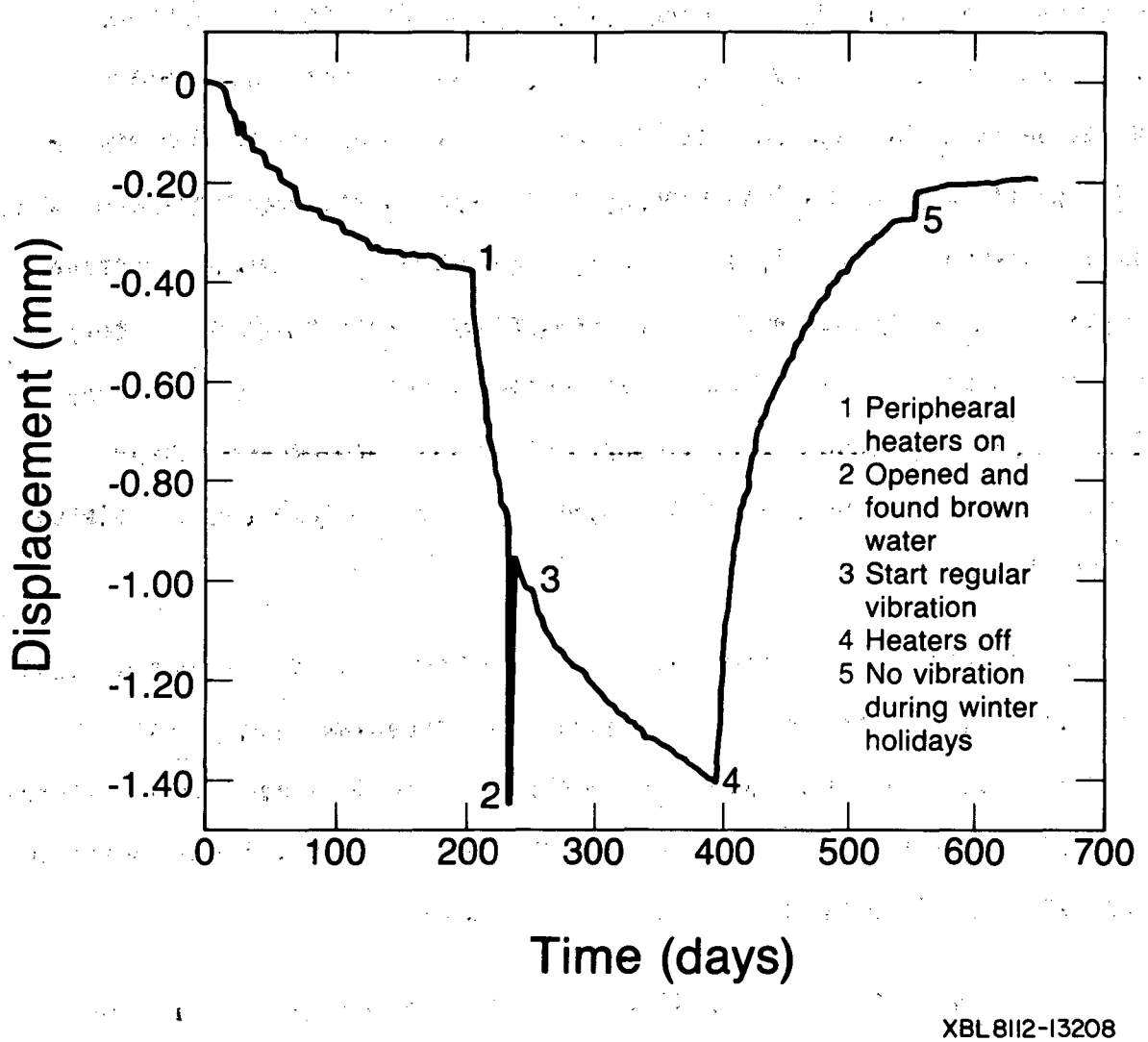

Fig. 15. Displacement record for extensometer E29A.

the leads, and waterproofing the solder joint with shrink tubing and tape. Because the sensors were so reliable, the quick change characteristics of an exposed screw connection were not required. The power supply and sensor outputs were grounded, which made them less susceptible to common-mode electrical noise. The negative side of the sensor power supply was also connected to ground through a 1 kΩ resistor.

Despite all these changes, some signals continued to be noisy, but the source was not identified. However, when several sensors were recovered for laboratory tests after 2 years of field operation, they operated as well as when they were first installed in the field, i.e., with noise-free and reproducible output.

The water leakage was thought to have been caused by the thermal relaxation of a gasket (described in Section 3.3 above), inadequately sealed pipe threads, or installation damage to the silicon rubber sleeve. A more abrasion-resistant covering over the silicon rubber would reduce the probability of such damage.

4.0 FIELD CALIBRATION AND VERIFICATION

4.1 DCDT Calibration

The calibration technique recommended by the manufacturer (Terrametrics, 1977) was followed. This consisted of measuring the output voltages of each of the four DCDT transducers on a given extensometer while the head assembly was supported on three shims with precisely machined steps. By measuring the output voltage of each sensor at several shim heights (in 5-mm steps) and computing a least-squares linear fit to the data, a calibration constant (mm/V) was determined for each sensor.

Initially, the calibration constant was taken to be a linear fit to data for the full range of calibration steps; however, since the calibration data was slightly nonlinear over that range (Table 5) and since all extensometers operated within the voltage range of -1.5 V to 0.25 V, the calibration constants were subsequently reevaluated using the output voltages from the 5-, 10-, and 15-mm shim steps only. Over the displacement range used at Stripa, this nonlinearity contributed an error of less than 1% to the calculated displacement.

The calibration constant to be used for converting the raw data into engineering units was taken to be the average of the values from these 10-mm range measurements made before and after the experiment. These calibration constants (Table 6) varied from 2.09 to 2.56 mm/V, and 94% of them had values between 2.1 and 2.3 mm/V. Figure 16 shows a histogram for the percentage of change in the constants between 1978 and 1980. Most (92%) of the sensors changed their calibration constant by 2% or less, and the average

Table 5. Pre- and post-experiment calibration data for sensor E-1A. Comparisons between slopes at intermediate steps during the pre- and post-experiment calibration.

Pre-Experiment Calibration			Post-Experiment Calibration		
Shim Height (mm)	DCDT Output (V)	Local Slope (mm/V)	Shim Height (mm)	DCDT Output (V)	Local Slope (mm/V)
0	-5.9300		0	-5.8950	
		2.1436			2.1390
5	-3.5975		5	-3.5575	
		2.1505			2.1356
10	-1.2725		10	-1.2162	
		2.1930			2.1787
15	1.0075		15	1.0787	
		2.2272			2.2160
20	3.2525		20	3.3350	
		----			2.2779
25	no data		25	5.5300	

Table 6. Extensometer calibration constants.

Extensometer Code	Sensor Number	C [a] (mm/V)	Change[b] %	Extensometer Code	Sensor Number	C (mm/V)	Change (%)
Time Scale Vertical Extensometers							
E1 A	1081	2.1642	-0.7	E4 A	1093	2.1326	-0.8
B	1082	2.1209	0.0	B	1094	2.0910	-0.5
C	1083	2.1293	-0.6	C	1095	2.1086	-1.2
D	1084	2.1114	-0.7	D	1096	2.1198	-0.6
E2 A	1085	2.2026	-0.1	E5 A	1097	2.1167	-1.1
B	1086	2.1301	-0.5	B	1098	2.1153	-1.1
C	1087	2.1089	-0.2	C	1099	2.1114	-0.6
D	1088	2.1091	-0.4	D	1100	2.0959	-0.5
E3 A	1089	2.1224	-0.6				
B	1090	2.1116	-0.6				
C	1091	2.1271	-0.6				
D	1092	2.0940	-0.6				
H9 Vertical Extensometers							
E6 A	291	2.2055	-1.5	E9 A	303	2.1602	-1.3
B	292	2.1684	-1.3	B	304	2.1394	-1.2
C	293	2.1460	-1.3	C	305	2.1349	-1.4
D	294	2.1335	-1.8	D	306	2.1369	-1.4
E7 A	295	2.1412	-1.8	E10A	307	2.1987	-0.6
B	296	2.1503	-1.8	B	308	2.1436	-0.2
C	297	2.1337	-1.0	C	309	2.1589	-0.9
D	298	2.2112	-0.8	D	310	2.1220	-1.1
E8 A	299	2.2248	-1.6	E11A	311	2.3255	+0.5
B	300	2.1480	-0.9	B	312	2.4496	-0.1
C	301	2.1687	-0.8	C	313	2.2105	-0.1
D	302	2.1256	-1.5	D	314	2.5477	+0.1
H-10 Vertical Extensometers							
E12A	801	2.1934	-0.3	E15A	813	2.1966	+0.7
B	802	2.1867	-0.1	B	814	2.1147	-0.7
C	803	2.1212	-0.1	C	815	2.1339	+0.8
D	804	2.1046	+1.6	D	816	2.1206	-0.4
E13A	805	2.1781	-1.1	E16A	817	2.2387	-0.4
B	806	2.5602	-1.0	B	818	2.1533	-1.4
C	807	2.1359	-0.3	C	819	2.1514	+0.6
D	808	2.1266	-0.8	D	820	2.1627	-0.5
E14A	809	2.1816	+0.7	E17A	821	2.1532	+0.5
B	810	2.1243	+0.5	B	822	2.1197	-0.3
C	811	2.1204	+1.4	C	823	2.1238	+2.4
D	812	2.1294	+0.2	D	824	2.1265	+0.1

Table 6. Extensometer calibration constants (continued)

Extensometer Code	Sensor Number	C [a] (mm/V)	Change[b] (%)	Extensometer Code	Sensor Number	C (mm/V)	Change (%)
H9 Horizontal Extensometers							
E18A	315	2.1305	-1.7	E23A	335	2.1640	-1.1
B	316	2.1327	-1.9	B	336	2.1466	-1.3
C	317	2.1520	-1.0	C	337	2.1761	-1.7
D	318	2.1211	-0.4	D	338	2.1506	-0.9
E19A	319	2.1945	-1.1	E24A	339	2.1609	-1.6
B	320	2.1430	-2.0	B	340	2.1459	+0.2
C	321	2.1144	-2.1	C	341	2.1258	-1.2
D	322	2.1623	-1.6	D	342	2.1229	-0.6
E20A	323	2.1791	-1.3	E25A	343	2.1552	-1.2
B	324	2.1286	-1.6	B	344	2.1576	-0.8
C	325	2.1529	-1.5	C	345	2.1394	-1.5
D	326	2.1519	-2.0	D	346	2.1040	-1.6
E21A	327	2.1752	-0.7	E26A	347	2.1655	-1.6
B	328	2.1494	-0.6	B	348	2.1495	-1.2
C	329	2.1434	-1.3	C	349	2.1346	-1.5
D	330	2.1457	-3.5	D	350	2.1296	-1.9
E22A	331	2.1734	-1.2				
B	332	2.1476	-1.9				
C	333	2.1337	-0.9				
D	334	2.1345	-1.3				
H10 Horizontal Extensometers							
E27A	825	2.1659	-0.9	E31A	841	2.1622	-1.3
B	826	2.1651	-1.1	B	842	2.1637	-1.2
C	827	2.1383	-1.3	C	843	2.1590	-1.5
D	828	2.1356	-0.7	D	844	2.1177	-1.9
E28A	829	2.1538	-1.3	E32A	845	2.1640	-1.6
B	830	2.1585	-1.5	B	846	2.1468	-1.1
C	831	2.1327	-2.2	C	847	2.1492	-1.8
D	832	2.0916	-1.0	D	848	2.1269	-1.4
E29A	833	2.1442	0.0	E33A	849	2.1957	+0.4
B	834	2.1291	+0.3	B	850	2.1330	+0.3
C	835	2.1220	+0.2	C	851	2.1220	+0.5
D	836	2.1074	0.0	D	852	2.1271	+0.6
E30A	837	2.1806	-1.9	E34A	853	2.1760	+0.6
B	838	2.1808	-1.4	B	854	2.1602	-1.0
C	839	2.1477	-0.9	C	855	2.1394	-1.7
D	840	2.1451	-1.1	D	856	2.2737	+11.9[c]

Table 6. Extensometer calibration constants (continued)

Extensometer Code	Sensor Number	C [a] (mm/V)	Change[b] (%)
H10 Horizontal Extensometers (continued)			
E35A	857	2.1411	-0.4
B	858	2.1686	-0.4
C	859	2.1200	0.0
D	860	2.1086	-0.4

[a] C = calibration constant proposed for data reduction = $[C_{1978} + C_{1980}] \div 2$,
where C_{1978} = calibration constant as measured in the summer of 1978 for the 5, 10, and 15 mm shim position only.
C_{1980} = calibration constant as measured in the spring of 1980 for the 5, 10, and 15 mm shim position only.

[b] Percent change = $[(C_{1980} - C_{1978})/C_{1978}] \times 100$.

[c] DCDT coils were switched between sensors 332 and 856 on 9/21/79.

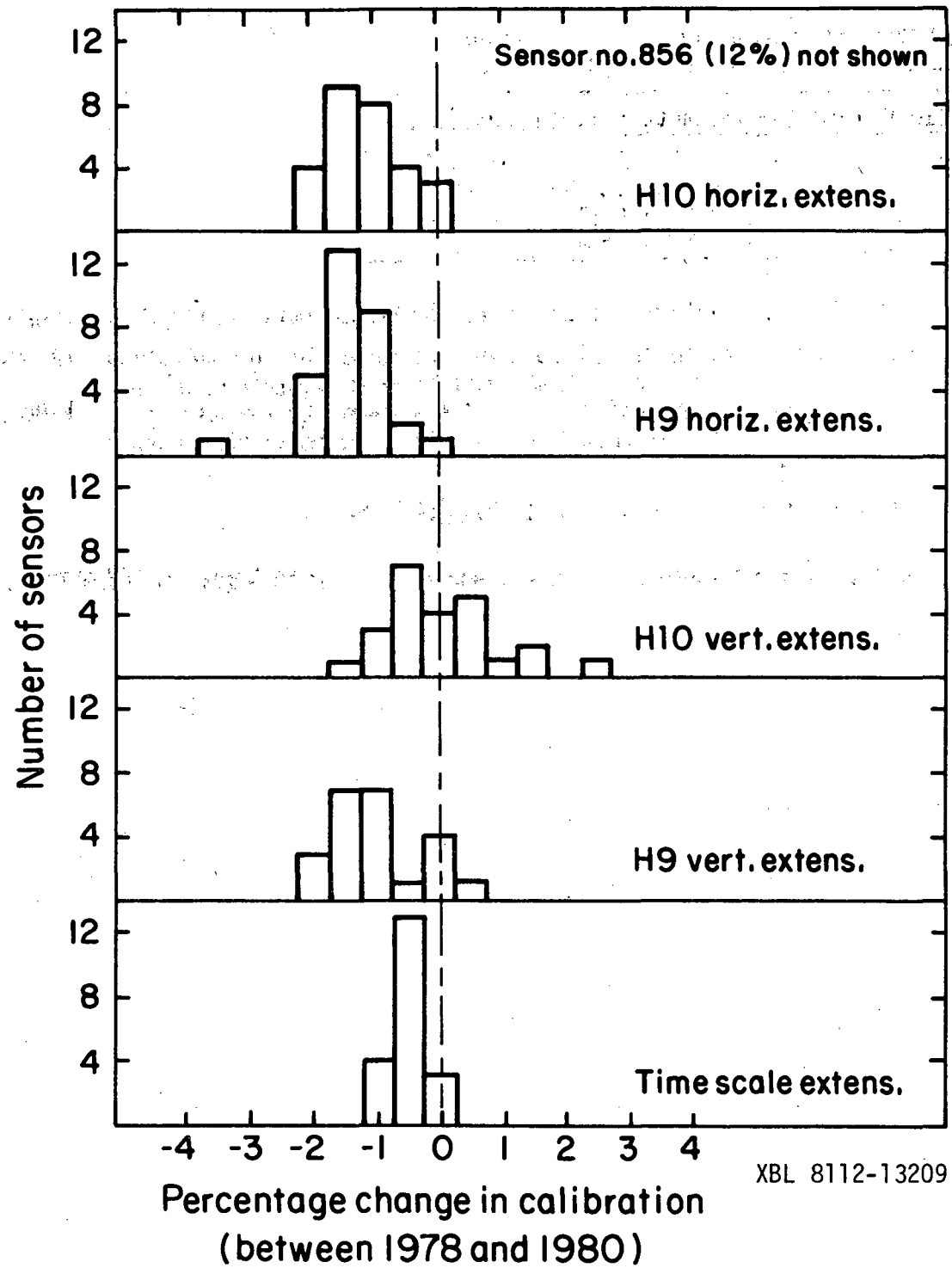

Fig. 16. Histogram of changes in calibration.

change was -0.8%. A 2% change in calibration, when evaluated over the 3-mm maximum response, is equivalent to a 60-μm change in displacement.

The standard calibration technique requires that the head be lifted by advancing each jacking screw (three at 120°) until three precision shims can be placed under the head. Then, by retracting each screw, the head is lowered onto the shims. Because of rod friction and friction in the head assembly, and because of tilting of the head while being raised and lowered by the three screws, the calibration is not a perfect simulation of normal extensometer operation. By using a gear-driven system to synchronize the three jacking screws, the tilting could be eliminated and the head motion could be made continuously in one direction. Our experience with such a tool is described in Section 5.

4.2 Circuit Verification

After completion of the post-experiment calibration, the position of each DCDT coil was manually adjusted so that each coil provided a unique output voltage. This voltage was measured with a portable voltmeter directly across the DCDT leads. Subsequently, the output of each DCDT was recorded by the data logger and by the computer. These three sets of output voltages were compared to verify that all agreed as to the correspondence between the voltages and their associated sensor numbers. The comparisons confirmed that the data loggers and the computer had been correctly identifying these sensors.

4.3 Anchor Verification

As an extension of the effort to assure that the recorded data was identified with the appropriate sensor system, we attempted to verify the correspondence between each DCDT sensor number and the corresponding

extensometer anchor depth as recorded during installation. A rod normally operates under an axial load of about 500 N, applied by a tensioning spring mounted in the head assembly. Using a simple lever, each extensorod was pulled with an aditional axial force of about 450 N. This test approximately doubled the rod stress to a total of 29 MPa (roughly 10% of the yield strength of Superinvar). The resulting extension of the rod caused a change in the DCDT output voltage. The elastic stretch of the rod, and the DCDT voltage change, should be proportional to the rod length. The response of each of the time-scaled vertical extensometer rods to this tensile loading was approximately 30% greater than the 0.1 mm/meter of rod length that would be expected for a straight rod when using the manufacturer's value (148 GPa) for the Young's modulus of Superinvar. The incremental tension would have tended to straighten out any bends or catenary sags in the rod, and this straightening may have been responsible for the larger-than-expected sensor response.

Even with scatter in the data, the responses from the rod-pull tests on extensometers E1 through E5 confirmed the relative anchor depths as recorded at installation. A similar response and verification was observed for the single-rod pull tests performed on vertical extensometers in the H9 and H10 areas.

The data from pull tests on the horizontal extensometers showed greater scatter, and, in eight cases, these tests failed to corroborate the relative rod lengths recorded at installation. However, this pull test was very difficult to perform on most of the horizontal extensometers

because of the angle at which they were installed and because of their elevation above the floor of the drift. Repeating the test for these eight cases did not yield reproducible results. The test was therefore not considered to be reliable for identifying the relative lengths of the horizontal rods. An additional characteristic of the horizontal extensometers which contributes to this difficulty is that most of the rods are longer than those for the vertical extensometers but the ratios between the lengths of the four rods within a given borehole are smaller than for the vertical extensometers. In several cases, adjacent horizontal rods vary in length by less than 10%.

4.4 Thermocouple Verification

For each borehole (at a time near the heater turn-off date), the temperature indicated by each extensometer thermocouple was plotted versus the recorded depth of that thermocouple. A smooth temperature profile curve was drawn through the data points for each E-hole, and these curves were inspected to determine if all thermocouples were functioning and if the resulting temperature profiles were reasonable. Thermocouple 501 on E35 was inoperative (it had been broken during extensometer installation). Thermocouple 126 on E13 indicated too low a temperature when it was checked at the conclusion of the cooldown period (about 70 days after heater turn-off). This error was found to result from a 7.5°C offset at its ice-point reference junction. The ice-point reference unit had been replaced on August 9, 1979. The thermocouple output did not change as a result of this replacement. From inspection of the output data, it seems probable that the 7.5°C offset developed

gradually over the final 298 days of the experiment. Two vertical extensometers showed unusual temperature profiles because of water leakage, as discussed in Section 3.30.

The extensometer temperature profiles also revealed two cases in which the thermocouple depths, as recorded in Schrauf et al. (1979), appeared to be interchanged. This hypothesis was verified by measuring the resistance of the thermocouple leads in question. The instrumentation listing in Chan et al. (1980) shows the corrected locations for these thermocouples.

5.0 LABORATORY TESTS

5.1 General

As noted, it became evident within the first 100 experiment days that many DCDT sensors were responding in a stepwise fashion (Hood, 1979). We suspected that the extensometers were demonstrating frictional stick-slip. To test this hypothesis, and to evaluate the magnitude and causes of any such friction, a simplified mock-up of a horizontal extensometer was tested in the laboratory. These tests and the extensometer vibration tests at Stripa (Section 3.5) indicated that friction within the instrument was the primary cause for stepwise changes in the displacement record. A second and more complete mock-up of a horizontal extensometer subsequently confirmed this conclusion and provided additional understanding of the sources of friction.

These laboratory tests evaluated the impact of several variables upon the indicated displacement resulting from a specific pattern of anchor motions; they also compared the sensor output resulting from anchor motion with that resulting from head motion (as used for field calibration). The head motion was provided by a new tool that could provide a smooth displacement in very small increments. These laboratory tests and the tool are described below, and the laboratory test results are discussed as an aid to interpreting the performance of the Stripa extensometers.

5.2 Description of Extensometer Mock-Up

Both laboratory extensometer mock ups were installed in a horizontal configuration because it was assumed that the resulting gravitational

loading on the horizontal rods would create the conditions for maximum friction and because access to the various parts of the assembly could not conveniently be provided if such a long assembly was mounted vertically.

Both mock-ups used four simulated anchors and a flexible conduit between anchors; however, the conduit was not grouted. To simulate the constraint of the borehole wall, a support was placed under the conduit at the appropriate height.

In the first mock-up, the axial position of only the deepest anchor was adjustable. It had a threaded adjusting ring. Although four anchors and tensioned rods were installed, only the longest rod was equipped with a displacement sensor. The rods were 6.1, 7.9, 9.2, and 10.4 m long. The internal dimensions of the simulated anchors were identical to those of the Stripa anchors.

A photograph of the second mock-up is shown in Fig. 17. The anchor locations and rod lengths are shown in Fig. 18. The simulated anchors (Fig. 19), were mounted in brackets bolted to the heavy concrete floor of the laboratory. Each bracket was equipped with alignment pins to prevent anchor rotation and with an adjusting ring that had differential pitch threads for fine adjustment of the axial location of the anchor. The ring was rotated by a spanner wrench, and its rotary movement was monitored by counting the number of notches (gear teeth) that passed a fixed fiducial mark. A rotation of one notch produced an axial displacement of 2.20 μm.

The extensometer was equipped with four DCDT sensors that had been removed from the Stripa time-scaled experiment extensometers after the

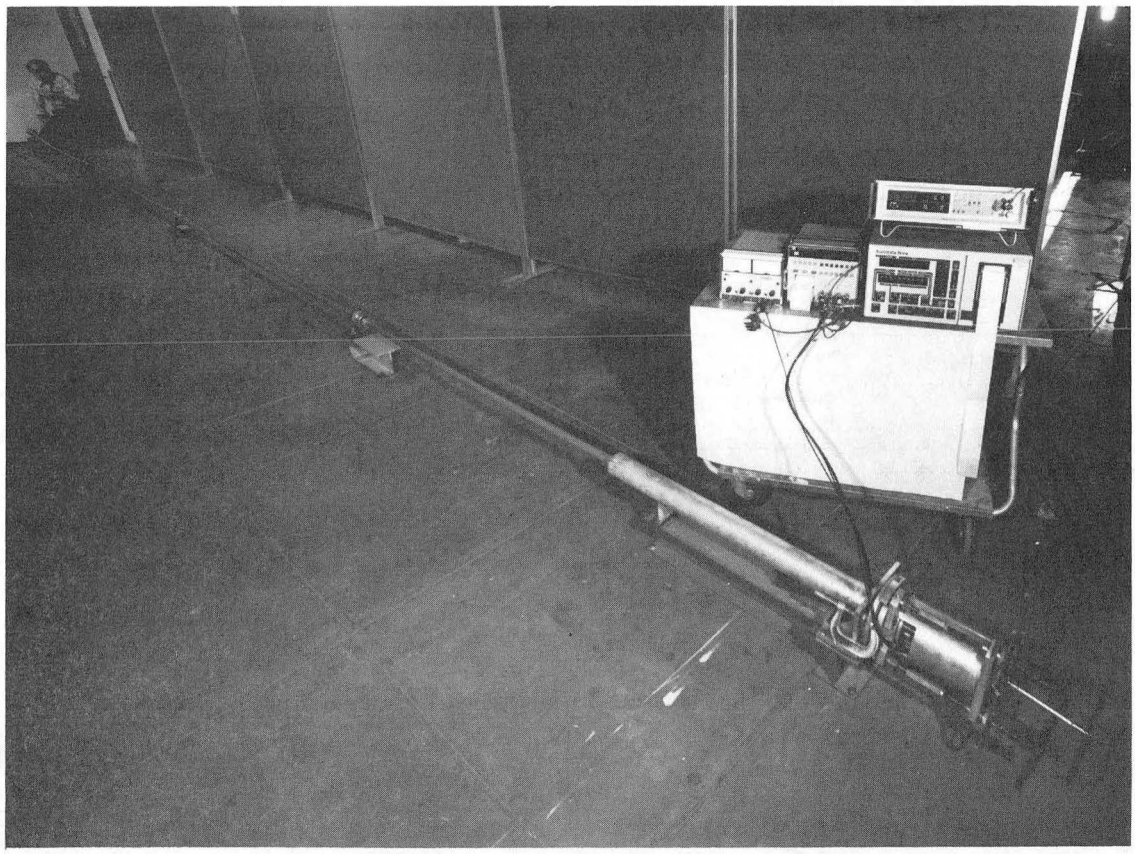

CBB 812-1483

Fig. 17. Laboratory mock-up of a horizontal extensometer.

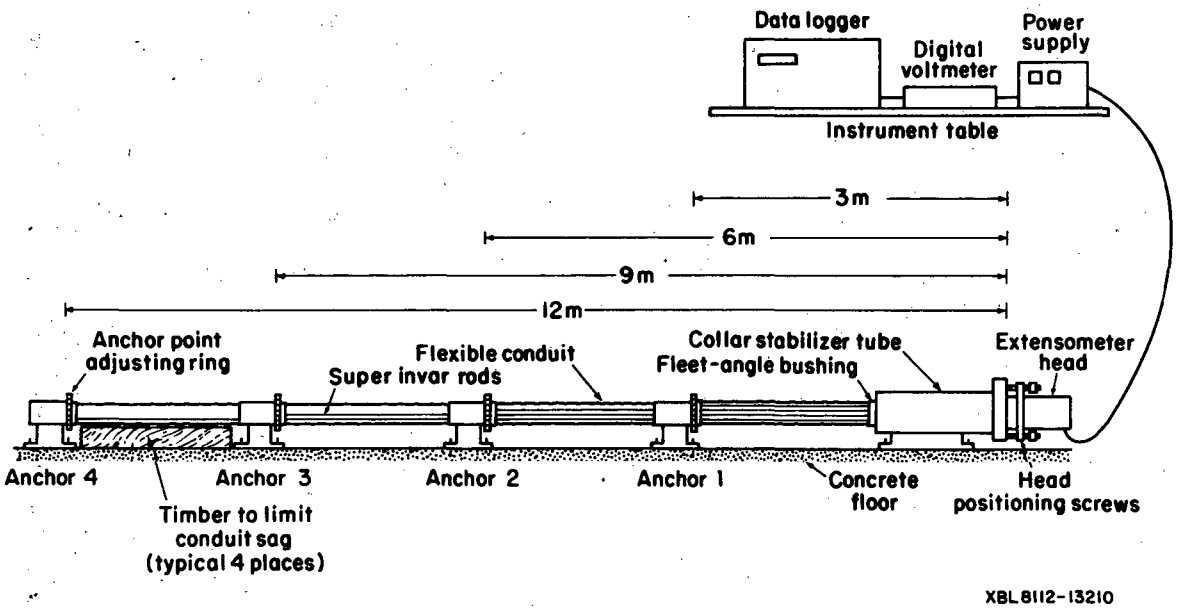

Fig. 18. Schematic arrangement of the laboratory apparatus.

CBB 812-1489

Fig. 19. Operation of an adjustable anchor.

post-experiment calibrations were completed. These sensors were instrumented as shown in Fig. 17 and were powered by a Hewlett-Packard 6227B dual DC power supply operating at 10.19 ± 0.001 V. Each sensor was mounted so as to provide an output voltage of -1.25 to 0.05 V at the zero displacement position of its anchor. All voltages were monitored by a Fluke 8500A digital multimeter. The sensor output voltage, time of day, and room temperature were recorded by an Accurex Autodata Nine datalogger.

For both the Stripa and laboratory extensometers, the positions of the rod anchor points around the anchor centerline were chosen to encourage the four rods to pass from anchor to head in straight parallel paths. The threaded end of each rod was attached to a threaded socket welded to the inside wall of its anchor. The threaded socket on the shallowest anchor was located at 12 o'clock (top dead center). Each subsequent socket was indexed by 90° counterclockwise, as viewed from the head. The rods remained in this relationship to each other as they passed through the fleet-angle bushing and the spring-loaded guide tubes. This arrangement was used at Stripa and for mock-up 2. For the earlier mock-up, the rods were arranged in the same rotation; however the entire pattern was rotated 90°, with the shallowest anchor socket at 3 o'clock and the deepest at 12 o'clock.

5.3 Description of Microadjuster

The standard head-positioning technique for calibrating an extensometer in the field (Section 4.1) has some drawbacks, especially when attempting to isolate frictional effects. To avoid these drawbacks, a special tool which we call a microadjuster, was constructed. The microadjuster will

raise or lower the head without tilting it and can raise or lower the head by very small and reproducible increments.

This tool is shown schematically in Fig. 20; Fig. 21 shows it in operation. The instrument is attached to the extensometer head; with three screws at 120°, it pushes against the face of the collar stabilizer flange.

The operator rotates a center drive pinion that simultaneously rotates three satellite gears. Each satellite gear rotates a push screw. Each push screw has two threaded sections--a coarse-pitch thread that engages a nut secured in the microadjuster body and a fine-pitch thread that engages a nut pressing against the collar stabilizer flange. This differential-pitch system provides a net axial motion of 0.94 μm for each one-tooth rotation of one of the three large (80-tooth) gears. Because of variations in the thread pitches, the microadjuster operates with a slight sinusoidal variation in its nominally linear motion.

5.4 Test Procedure for First Mock-Up

The deepest anchor was equipped with an axial position adjustment ring with a 20 pitch thread (20 revolutions per inch of travel). The adjustment ring was first rotated 90° in the direction to simulate rock compression, and then rotated back to the fiducial mark, to store friction in the assembly equivalent to that which would result from rock extension. A reading of the DCDT output voltage was recorded and the procedure repeated several times so that an average output voltage could be calculated. The same procedure was repeated with the

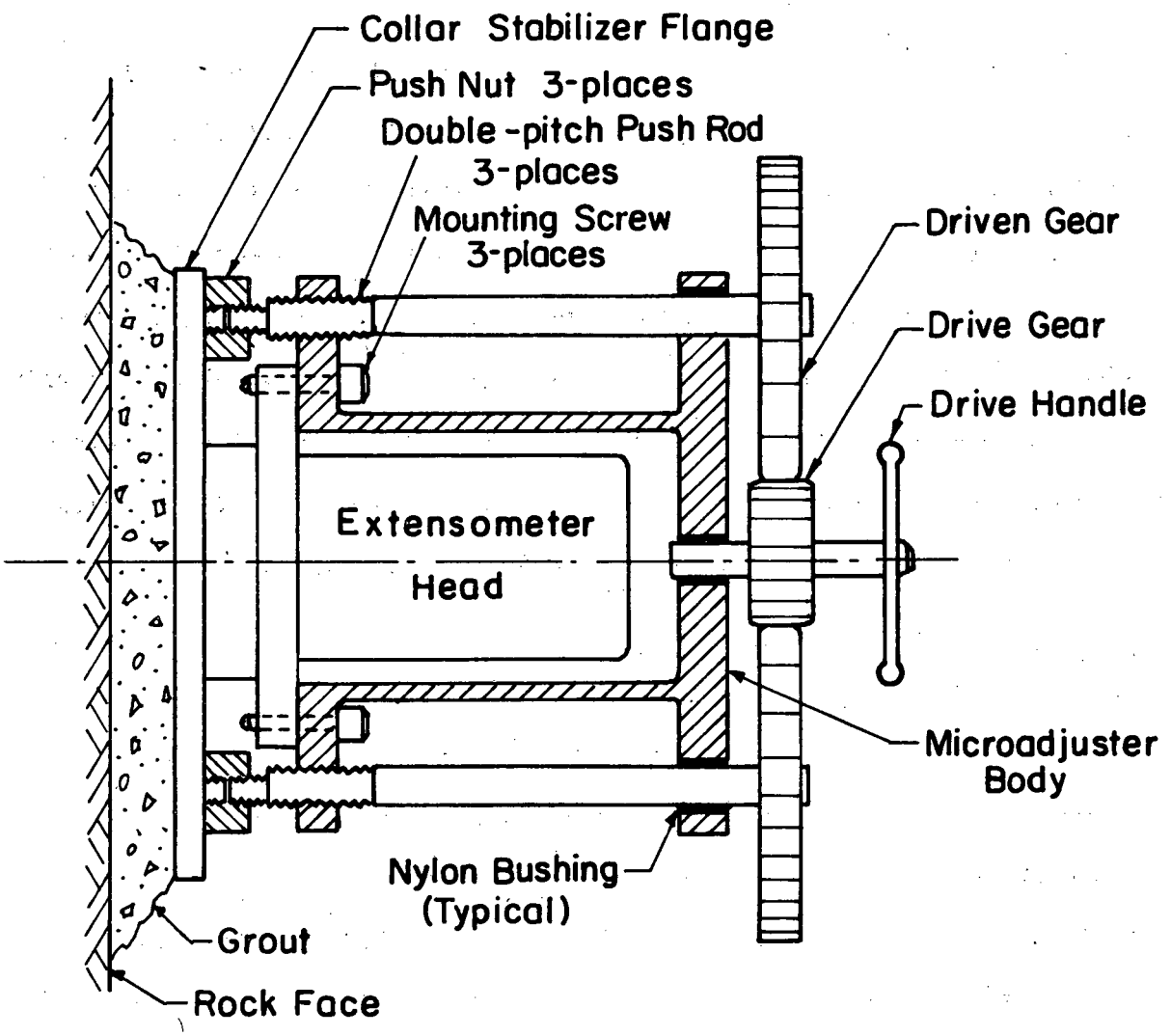

Fig. 20. Schematic of the microadjuster.

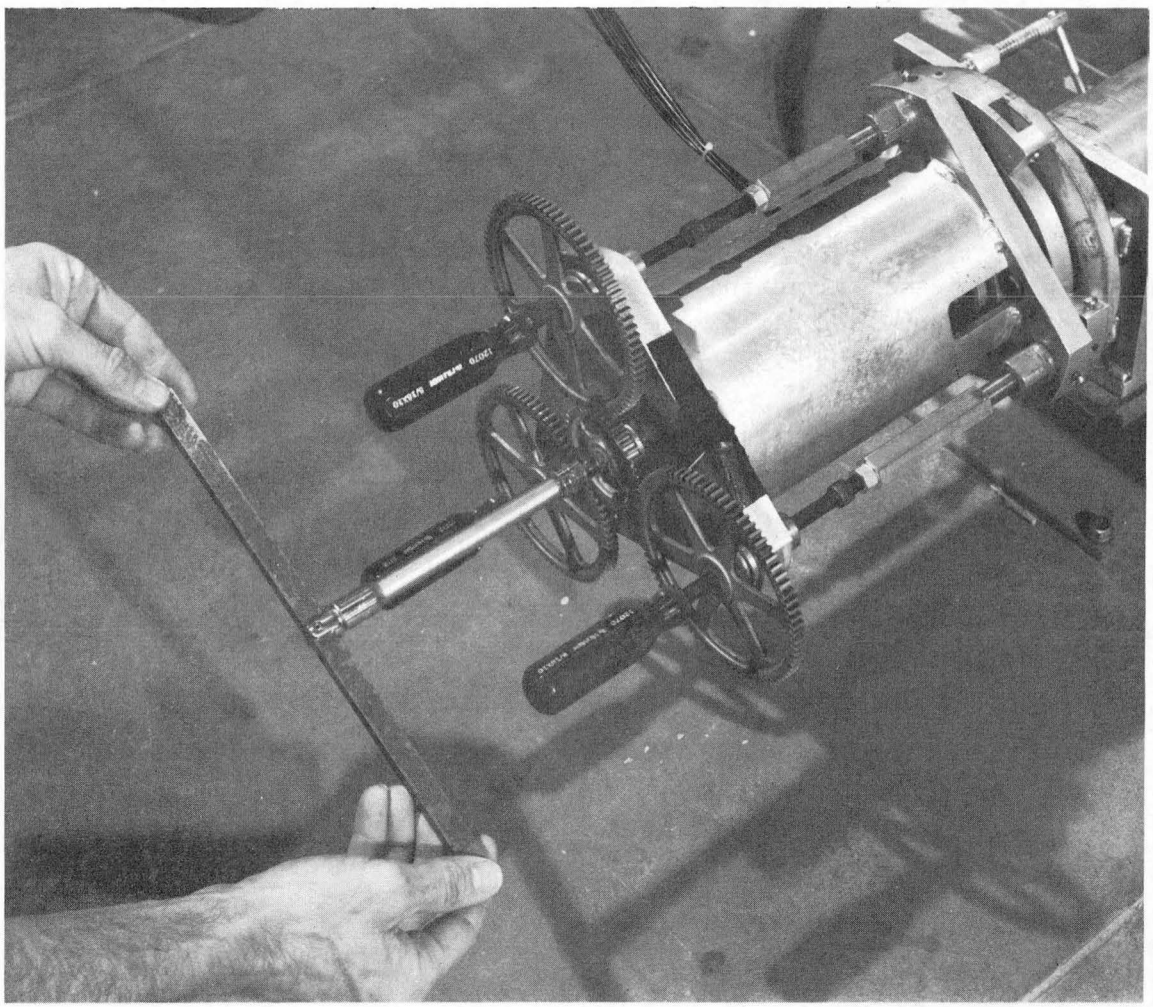

CBB 812-1487

Fig. 21. Operation of the microadjuster.

rotation reversed--i.e. first rotation of the adjusting ring on the anchor to simulate extension and then back to the fiducial mark to store friction equivalent to that resulting from compression.

The difference between the output voltage readings that resulted from these two adjustment patterns was taken to represent the frictional lag that could be stored as a result of a reversal in displacement. By comparing the average responses from five repetitions of each reversal, the uncertainty resulting from the coarseness of the adjusting thread was mitigated. The effect of several parameters were evaluated using this displacement reversal technique on the deepest anchor.

5.4.1 Conduit

The test was performed with and without the flexible conduit installed around the rods. When the conduit was removed, the conduit adapter fittings were removed as well.

5.4.2 Anchor Alignment

Before the tests described here, one of the standard hydraulic flatjack anchors was placed into a 3-inch, schedule 40 steel pipe (to simulate a Stripa borehole) and the anchor was inflated to 14 MPa (2,000 psi). As the flatjack was inflated, it drove the anchor toward one side of the hole (Fig. 6). The anchor centerline was then about 5 mm off the axis of the hole. Because of this result, we decided to misalign each anchor of our mock-up by 5 mm for one test and by 10 mm for a second test. The 10-mm misalignment was intended to evaluate the effect of a borehole that was not perfectly straight.

5.4.3 Conduit Support

Tension in the flexible conduit was established during the installation of the extensometer. This tension, the flotation from the grout, and ultimately the borehole wall all participate in determining the pattern of conduit sag and the amount of normal force between the conduit and the rods. Tests were done in three configurations: (1) with no support for the conduit, (2) with the sag limited to 21 mm (equivalent to the constraint of a borehole), and (3) with an upward force of 15 N/m (exerted by a sponge-rubber pad) to simulate the flotation effect of grout. In all cases, only the 5.1-m-long catenary between the shallowest anchor and the head was supported or loaded by the sponge rubber. The catenaries between the other anchors were quite small because of their short spans.

5.4.4 Rod and Anchor Orientation

The rod positions within the conduit were varied from the arrangement described above--active rod at 12 o'clock--to an arrangement with the entire system rotated 180° so that the active rod was at 6 o'clock.

5.4.5 Vibration

All of the above installation parameters were evaluated with and without vibration of the head assembly and one (or more) of the anchors. The vibration was induced by tapping, up to 50 times, with a 25-mm-square by 150-mm-long aluminum rod.

5.5 Test Results from First Mock Up

The hysteresis observed during the simulated extensometer operations on the first mock-up is tabulated in Table 7 and Table 8. Table 7 lists the

Table 7. Test results from first laboratory mock-up.

Test Suite Code	Was Conduit Installed?	Was Conduit Supported?	Anchor Misalign (mm)	#4 Rod Position[a] (o'clock)	Vibration		Total Hysteresis (μm)
					Head	Anchors	
a1	No	--	0	12	No	No	33
2					Yes	No	9
b1	No	--	10	12	No	No	42
2					Yes	No	8
3					Yes	Yes	1
c1	Yes	No	0	12	No	No	175
2					Yes	No	123
3					Yes	Yes	80
d1	Yes	Yes	0	12	No	No	148
2					Yes	No	96
3					Yes	Yes	21
e1	Yes	No	0	6	No	No	129
2					Yes	No	90
3					Yes	Yes	34
f1	Yes	15 N/m	0	6	No	No	130
2					Yes	No	76
3					Yes	Yes	30
g1	Yes	Yes	5	12	No	No	182
2					Yes	No	126
3					Yes	Yes	49
h1	Yes	15 N/m	5	12	No	No	139
2					Yes	No	92
3					Yes	Yes	52
i1	Yes	No	5	b	No	No	136
2					Yes	No	83
3					Yes	Yes	61
j1	Yes	15 N/m	5	b	No	No	150
2					Yes	No	113
3					Yes	Yes	106

[a] Only #4 Rod (10.4 m long) was instrumented.
[b] Anchors #2 and #4 rotated about their axis 90° opposite directions; remainder of assembly was unchanged.

Table 8. Effect of specific variables upon test results from the first mock-up. The effects are highlighted by comparing pairs of test suites for which a single parameter is changed. Tabular values given are the total measured hysteresis for the longest rod, in units of μm. Values are given for three test procedures: (1) no vibration, (2) only the head vibrated, and 3) both the head and one or more anchors vibrated.

	Test Suite	Parameters	Vibration None (1)	Head (2)	Both (3)
Conduit versus No Conduit					
Anchors well aligned	a	No Conduit	33	-9	No Data
	c	Conduit, unsupported	175	123	80
		Net Change (c - a)	142	132	--
	a	No Conduit	33	-9	No Data
	d	Conduit, neutral support	148	96	21
		Net Change (d - a)	115	105	--
Conduit Support					
Anchors well aligned with normal rod positions	c	No Support	175	123	80
	d	Neutral Support	148	96	21
		Net Change (c - d)	27	27	59
Anchors well aligned with rods inverted	e	No Support	129	90	34
		/m upward force	130	76	30
		Net Change (e - f)	-1	14	4
Anchors misaligned 5 mm with normal rod position	g	Neutral Support	182	126	49
	h	15 N/m upward force	139	92	52
		Net Change (g - h)	43	34	-3
Anchors 2 and 4 rotated out of position with all anchors misaligned 5 mm	i	No Support	136	83	61
	j	15 N/m upward force	150	113	106
		Net Change (j - i)	14	30	45
Anchor Alignment					
Normal rod position with no conduit	a	well aligned	33	-9	No Data
	b	misaligned 10 mm	42	8	1
		Net Change (b - a)	9	17	--
With conduit and normal rod position	d	well aligned	148	96	21
	g	misaligned 5 mm	182	126	49
		Net Change (g - d)	34	30	28
Rod Orientation					
Conduit unsupported	c	#4 rod at 12 o'clock	148	96	21
	e	#4 rod at 6 o'clock	129	50	34
		Net Change (c - e)	19	6	-13
Conduit supported	d	#4 rod at 12 o'clock	148	96	21
	f[a]	#4 rod at 6 o'clock	130	76	30
		Net Change (d - f)	18	30	-9
Rotational Tangling of Rods					
Conduit supported, anchors misaligned 5 mm	g	Anchors & rods aligned	182	126	49
	j[b]	#2,4 anchors rotated 90°	150	113	106
		Net Change (g - j)	32	13	-57

[a] Note that in this suite, the conduit is loaded upward by 15 N/m rather than under neutral support as for the other suite, in the set.

tests in the order performed and identifies the conditions. Each test is identified by a lower case letter plus a number. The letter identifies a given set of geometric parameters and the number 1, 2, or 3 denotes whether or not the head and/or the anchor was vibrated. Table 8 summarizes the results in a format which highlights the effects of each test variable and will be discussed in a later section.

5.6 Test Procedure for Second Mock Up

The standard test procedure was to rotate each of the four anchor adjusting rings by 10 divisions (equivalent to 22.05 μm of anchor displacement) in the direction simulating rock extension and then to read the output voltage from each of the four displacement sensors. Multiplying each output voltage by its gauge calibration factor yielded the indicated displacement for comparison with the actual anchor displacement (Fig. 22). This process was repeated until a total motion of 441 μm had been accumulated on each anchor. The motion was then reversed (simulating rock compression) in 20 steps until the original anchor positions were reached.

These procedures were repeated for each of ten sets of test parameters. In this way, the impact of each parameter could be evaluated. The sensor response versus anchor motion was plotted for each sensor and for each set of test parameters. These graphs are presented as Appendix A. The effects of each set of parameters upon extensometer friction was evaluated by comparing the total hysteresis observed for a complete cycle of extension and compression. The procedures used for investigating the various parameters are described below.

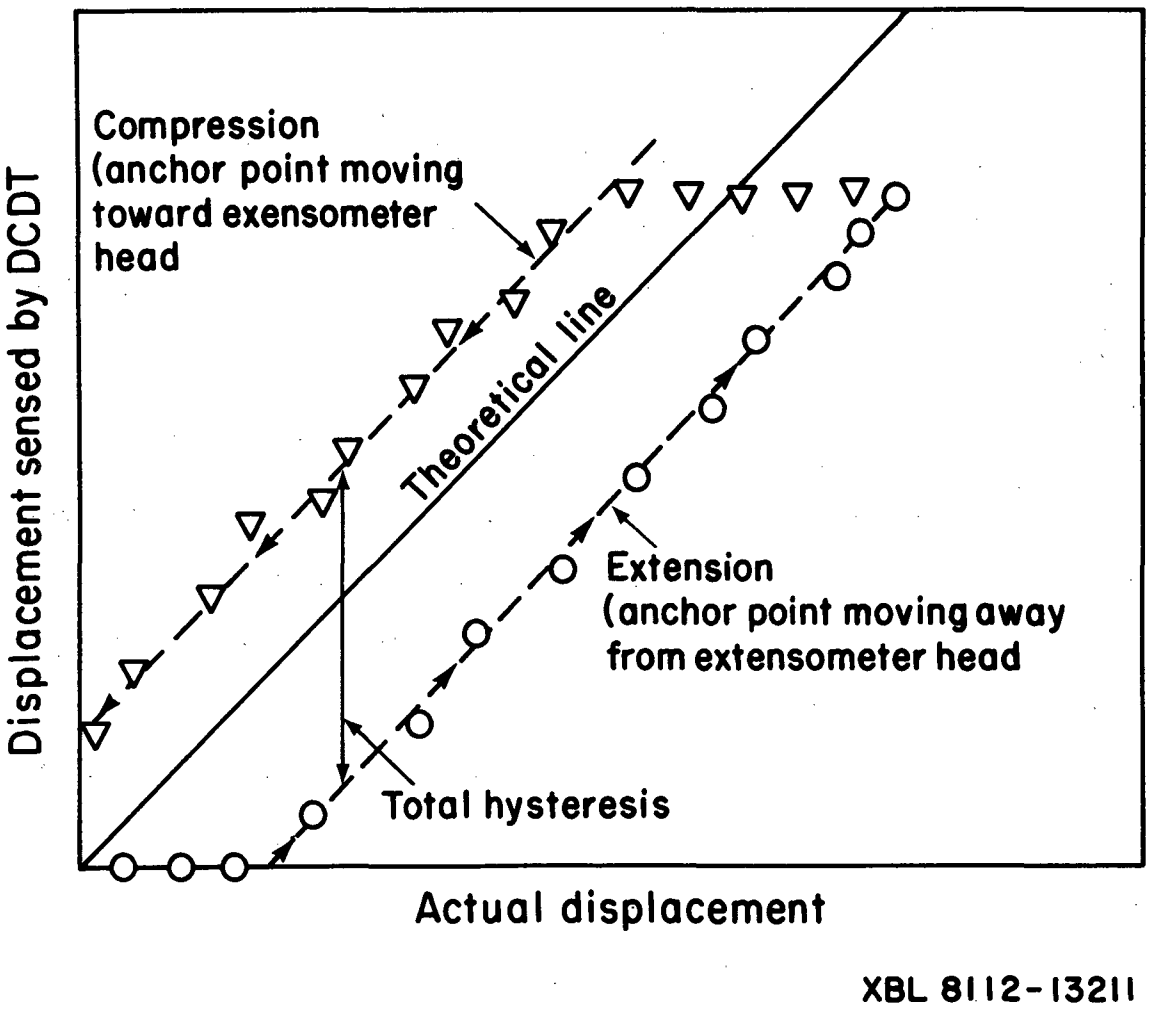

Fig. 22. Typical pattern of extensometer response during tests of second mock-up.

5.6.1. Conduit Support

All test suites except B and D were performed with a wooden timber supporting three of the four spans of flexible conduit. The timbers were positioned to limit the conduit sag to 21 mm, the amount that could occur within a 75-mm-diameter borehole. The short span (1.5 m) between the collar stabilizer tube and the first anchor sagged less than 10 mm--not enough to require one of these timbers. If unsupported, the conduit between anchor 1 and 2 sagged 25 mm; between anchor 2 and 3, it sagged 30 mm; and between anchor 3 and 4, 35 mm.

5.6.2. Rod and Anchor Orientation

Two orientations were tested. During most tests, the anchors were oriented so that the rod attachment sockets for adjacent anchors had the normal 90° of azimuthal separation; the shallowest anchor socket was oriented at 12 o'clock. To evaluate an installation geometry that might increase the interference between rods, test suites G and H were performed. In these two suites, the anchors were oriented so that all rod attachment sockets were at 6 o'clock. In all cases, the normal head orientation was maintained.

5.6.3. Number of Anchors

Test suites E and F were performed with the #1 and #2 anchors removed. The span from the collar stabilizer tube to the #3 anchor was fitted with a long piece of flexible conduit. Rods #1 and #2 were left inside the conduit and attached to the extensometer head. In these two suites, the #3 and #4 rods were at their normal length; however, the #3 rod passed through no anchors and the #4 rod passed through only one anchor.

5.6.4. Rod Length

The arrangement described above, in which the #1 and #2 anchors were removed, provided an opportunity to compare the relative amounts of hysteresis for a long and a short rod, both of which passed through no intervening anchors, i.e., #3 rod in this special arrangement versus #1 rod in the normal arrangement. A similar comparison can be made for long and short rods passing through one anchor (#4 rod in this special arrangement versus #2 rod in the normal arrangement).

5.6.5. Displacement of Head Versus Displacement of Anchors

In test suites I and J, the rock strain was simulated by using the microcalibrator to move the head. In all other tests, the rock strain was simulated by moving each of the four anchors in identical steps.

In both cases, a precursor displacement equivalent to rock compression was induced prior to recording the "zero displacement" output voltage from each of the four displacement sensors. All tests were also identical in that the stepwise displacements were taken first in the direction of rock extension and then in the direction of rock compression to the starting point. When a test was continued with a second cycle of extension and compression, the sensor response repeated that of the first cycle.

The microadjuster was advanced in displacement steps of 29.4 μm (equivalent to one-eighth of a revolution of the 80-tooth gears). The total motion in each direction was 470 μm.

5.6.6. Vibration of the Extensometer Head

As shown in Table 9, most of the other variables were evaluated both with and without vibrating the extensometer head. For each set of test conditions, a full displacement cycle without vibration would be repeated with vibration.

The four output voltages were recorded after each displacement step, the head was vibrated, and the voltages were again recorded before proceeding to the next displacement step. In each case, the vibration was induced with three strokes of a rubber-tipped hammer, from each of three directions, to simulate the routine used at Stripa after March 14, 1981.

5.7 Test Results from Second Mock-up

The results from operation of the second mock-up are shown in the 40 graphs included as Appendix A. Each graph represents the output of one sensor for one set of conditions. Each graph is identified according to test suite by letter (upper-case letters in this series) and the sensor/rod/anchor number. The conditions for each suite are identified in Table 9.

5.8 Discussion of Laboratory Test Results

The two mock-ups were different enough that their responses are not exactly comparable. However, they both confirm that: (1) internal rod friction can have a marked effect upon the response of an extensometer; (2) the details of the installation geometry are important in minimizing friction; and (3) vibration of the extensometer head can remove some, but not necessarily all, of the frictional effects. Observations on the effect of each installation and operating parameter are discussed below and summarized in Table 10.

Table 9. Test results from second laboratory mock-up.

Test Parameters						Total Hysteresis, μm			
						Rod Number, length			
Test Suite	Active Anchor	Conduit Support	Anchor Orientation (o'clock)	Displacement Induced at	Vibrate Head	1 3 m	2 6 m	3 9 m	4 12 m
A	All	Yes	Normal	Anchor	No	33	101	114	177
B	All	No	Normal	Anchor	No	33	115	122	384
C	All	Yes	Normal	Anchor	Yes	10	64	13	67
D	All	No	Normal	Anchor	Yes	10	64	18	45
E	3 & 4	Yes	Normal	Anchor	No	--	--	83	152
F	3 & 4	Yes	Normal	Anchor	Yes	--	--	17	43
G	All	Yes	All at 6	Anchor	No	16	184	--	206
H	All	Yes	All at 6	Anchor	Yes	7	94	--	47
I	All	Yes	Normal	Head	No	31	51	34	33
J	All	Yes	Normal	Head	Yes	13	13	18	19

Table 10. Effects of specific variables upon the test results from the second mock-up. The effects are highlighted by comparing pairs of test suites for which a single parameter is changed. Tabular values given are the total measured hysteresis in units of μm.

	Test Suite	Parameters	Rod Number 1	2	3	4
Conduit Support						
Without vibration	A	Neutral Support	33	101	114	177
	B	No Support	33	115	122	384
		Net Change (B - A)	0	14	8	207
With vibration	C	Neutral Support	10	64	13	67
	D	No Support	10	64	18	45
		Net Change (D - C)	0	0	5	-22
Rod Orientation						
Without vibration	A	Normal Orientation	10	64	13	67
	G	All rod sockets at 6 o'clock	16	184	--	206
		Net Change (G - A)	-17	83	--	29
With vibration	C	Normal Orientation	10	64	13	67
	H	all rod sockets at 6 o'clock	7	94	--	47
		Net Change (C - H)	3	-30	--	20
Number of Anchors Through Which a Rod Passes						
Without vibration	A	All anchors in place	--	--	114	177
	E	Anchors 1 & 2 removed	--	--	83	52
		Net Change (A - E)	--	--	31	125
With vibration	C	All anchors in place	--	--	13	67
	F	Anchors 1 & 2 removed	--	--	17	43
		Net Change (C - F)	--	--	-4	24
Variable Rod Lengths for a Constant Number of Anchors Encountered						
Without vibration	A	All anchors in place	33	101	--	--
	E	Anchors 1 & 2 removed	--	--	83	152
		Net Change (E - A)	--	--	50	51 [a]
Displacement induced by moving the head versus moving the anchors						
Without vibration	A	displace anchors	33	101	114	177
	I	displace head	31	51	34	33
		Net Change (A - I)	2	50	80	144
With vibration	C	displace anchors	10	64	13	67
	J	displace head	13	13	18	19
		Net Change (C - J)	-3	51	-5	48
Release of frictionally stored response by vibrating the head						
With Conduit Supported	A	no vibration	33	101	114	177
	C	with vibration	10	64	13	67
		Net Change (A - C)	23	37	101	110
With conduit supported/displacement at head	I	displace head/no vibration	31	51	34	33
	J	displace head/with vibration	13	13	18	19
		Net Change (I - J)	18	38	16	14

[a] Note that in this case the comparison is between A1 vs E3 and A2 vs E4.

5.8.1 Conduit

The tests with and without flexible conduit surrounding the rods were performed to confirm our suspicion that the constraint introduced by the conduit added significantly to the total hysteresis.

This suspicion is confirmed by the data in Table 8, where test suite c-1 (with conduit) showed a hysteresis increase of 142 μm over test suite a-1 (without conduit). The same table also shows that most of the incremental hysteresis remained after vibrating the head (Suite c-2); that even after vibrating both the head and the anchors (Suite c-3) much of the hysteresis remained.

We suspect that the friction added by the conduit would be much less for vertical extensometers. There would be no significant gravitational force generating loads between the rods and the conduit, or between the rods and the anchors, to create friction. Also, the rods would not sag between anchor points and therefore would not develop an inflection in their curvature at these support points. The constraint between the rigid straight bore of an anchor, with its conduit fittings, and the inflection in the curvature of a horizontal rod is probably the major cause of downhole friction.

A similiar comparison can be made for the case where the conduit is supported (Table 8). In this case, the frictional effects are increased by a smaller amount (115 μm); however, the general response is the same. Tests 2 and 3 of Suite d show that although anchor vibration can be more effective in releasing the friction if the conduit is supported, head vibration alone is unable to release all of the friction.

5.8.2 Conduit Support

The impact of conduit support upon the total hysteresis depends upon many factors, including the length of the span between anchors, the conduit tension, and the orientation of the axis with respect to gravity. Short spans and high conduit or rod tension may eliminate the possibility that a borehole wall will limit the sag or lift of the conduit.

The wet grout that was forced into the Stripa extensometer boreholes surrounded the conduit and provided a flotation effect on any horizontal conduit. This flotation force was resisted by the weight of the rods and by the borehole wall, which eventually limited the upward displacement of a horizontal conduit.

If one assumes that the effects of conduit tension are negligible, the maximum net buoyancy force transmitted by the conduit, against the rods or the upper borehole wall, is given by the following expression:

$$F = [\pi(d)^2\rho/4] - w$$

Where:

F = net unit buoyancy force, 11.5 N/m (0.783 lb/ft),

d = outside diameter of conduit, 0.0339 m (0.111 ft),

ρ = density of wet grout, 21,300 N/m^3 (136 lb/ft^3),

w = unit weight of conduit, 7.76 N/m (0.532 lb/ft).

The buoyancy force is 4.6 times the unit weight of a single rod (2.5 N/m). This buoyancy therefore could float a section of conduit containing even four rods. Under these circumstances, each section of conduit in a horizontal borehole will probably be displaced upward rather than downward.

In either case, the limiting deflection will be that permitted by the diameter of the borehole. As a result of this logic, the laboratory tests were primarily performed with the conduit sag limited to the maximum deflection--21 mm--possible within a 75-mm-diameter borehole.

The pertinent test suites from the first mock-up are summarized in Table 8. When support was provided, the friction was significantly reduced and this support improved the effectiveness of anchor vibration as a means of releasing much of the friction. Table 8 also shows that the effect of applying a 15 N/m upward force on the conduit will depend upon the details of the anchor alignment and the rod orientation within the conduit. The displacement of the conduit as a result of this upward force was not recorded.

The pertinent test suites from the second mock-up are sumarized in Table 10. Table 10 shows that the hysteresis for rod #4 was reduced dramatically (by 207 μm) when the conduit was supported. The #2 and #3 rods reacted much less to conduit support. The only segment of conduit through which the #1 rod passed had too small a sag to reach the support; therefore, this rod could not respond to the support.

5.8.3 Anchor Alignment

As discussed in Section 5.4, even if an extensometer is installed in a perfectly straight borehole, the anchor centerlines will be offset by about 5 mm as a result of the hydraulic bladder inflation. If the anchors are oriented so that the rod sockets on adjacent anchors are disposed 90° from each other, the progression of anchor sockets will describe a helix. The effect of this non-alignment in mock-up 1 is

summarized in Table 8. One can observe that the anchor offset has very little impact on the friction when no conduit is used. The anchor offset, with conduit, increased the hysteresis by 34 μm and the offset had little impact on the effectiveness of vibration in releasing the friction. Anchor misalignment was not tested on mock-up 2.

5.8.4 Rod and Anchor Orientation

The rotation of an anchor about its own axis changes the path of the rod which it anchors it also changes the friction between that rod socket and other rods passing through the anchor. The tests summarized in Table 8 illustrate, for mock-up 1, the effect that can result if the entire extensometer is rotated about its axis. In test suite e and f, the #4 rod is located at 6 o'clock (beneath all other rods), and this configuration results in slightly less hysteresis than for test suites c and d in which the #4 rod is located at 12 o'clock (on top of all other rods). Apparently, in this mockup, the friction created by ducking around other rod sockets when the #4 rod is at 12 o'clock, is more than that added by the drag of the rods lying on #4 when it is at 6 o'clock. No equivalent tests were performed on mock-up #1.

5.8.5 Number of Anchors

The tests summarized in Table 10 allow us to observe the changes in hystersis for rods #3 (-31 μm) and #4 (-125 μm) when they pass through two fewer anchors than they do in the normal four anchor installation. Suite E with fewer anchors shows a dramatic reduction in hysteresis. This response tends to confirm the hypothesis that much of the rod friction is created by the interference between the straight rigid bore of an anchor (and its conduit fittings) and the curvature of the rods as they pass through that anchor.

5.8.6 Rod Length

The tests summarized in Table 10 compare the hystereses recorded for rods of different lengths but passing through the same number of anchors to the extensometer head. In both cases (rod #3 vs. #1 and rod #4 vs. #2), we see about 50 μm greater hysteresis when rod length is increased by 6 m.

5.8.7 Vibration

Vibrating an extensometer head has been demonstrated to release some, but not all, of the rod motion that had been lockup up by friction. Table 10 clearly illustrates this. Note that, for the longer rods, greater amounts of hysteresis are stored and that, with vibration, a greater amount of hysteresis is released. This behavior results from the fact that a given frictional force creates an error in the indicated displacement that is proportional to the rod length. For example: an axial force of 25 N (5.6 lbs) would change the length of a 6.4-mm (0.25") diameter Superinvar rod by 5.4 μm per meter of rod length.

6.0 ERROR SOURCES

A formal error analysis has not been provided. A sensor-by-sensor analysis would be required since no two rods have experienced the same operating environment. There are, however, several factors that may contribute to an error in rock displacements calculated from the responses of the Stripa extensometers.

6.1 Displacement Sensor Calibration

The changes in displacement calibration constants were, for most sensors, within the range of ±2%. This calibration range was equivalent to displacement errors up to 62 μm. The special cases, identified in Table 6, would require individual evaluation.

6.2 Nonlinear Sensor Response

Nonlinearities in displacement sensor calibration did not exceed 0.5% over the operating range at Stripa. For the 2.1 mm maximum indicated displacement, this nonlinearity would result in an error of less than 11 μm.

6.3 Power Supply Voltage

The observed range of power supply voltage variations were equivalent to a maximum of 10 μm of displacement.

6.4 Rod Friction

Rod friction was demonstrated, by both laboratory and field tests, to be capable of causing wide variations in hysteresis. Vertical extensometers were shown in a field test to be capable of storing at least 81 μm of response in the longest rods and proportionally lesser amounts in the shorter rods.

Laboratory measurements demonstrated that horizontal extensometers might store as much as 177 μm of response in the longest rods and proportionally lesser amounts in the shorter rods. These maximum values are useful for evaluating instrument response before the practice of head vibration was instituted. The laboratory tests indicated that values less than one-third of these might be expected after head vibration was started.

6.5 Anchor Slip

We found no evidence of anchor slip, or of excessive anchor compliance.

6.6 DCDT Coil Slip

Some of the DCDT coils may have slipped as a result of set screws becoming loose during head vibration. The arbitrary changes in output voltage that would have resulted are not amenable to consideration here.

6.7 Young's Modulus

The maximum effect of thermal variation in Young's modulus for the Superinvar rods would probably not have exceeded 22 μm. This extreme case would only apply to a rod in the warmest zone surrounding the 5-kW heater. For all except the half dozen warmest rods, this thermal effect would have been negligible.

6.8 Thermal Strain

A single-best-fit table of values for thermal strain versus temperature was constructed on the basis of pre-experiment tests on seven Superinvar rods

(Schrauf et al., 1979). The range of values noted would allow an error of up to ±60 μm to be made in the calculation of the thermal expansion of the longest and warmest rod. A more typical error would be less than one-half of this value.

6.9 Thermocouple Temperature Calibration

The standard NBS limits of error are within ±2.2°C over a 20 to 160°C temperature range. A 2°C error in the temperatures of all of the thermocouples on the warmest and longest rod would result in an error of about 16 μm in the calculated thermal expansion.

7.0 CONCLUSIONS AND RECOMMENDATIONS

Thirty-five rod extensometers operated at Stripa throughout a two-year period and yielded an essentially continuous record of the displacements of 140 points within the rock mass. This operation demonstrated that these extensometers can function for an extended period in a damp environment at rock temperatures up to at least 150°C.

The inflated and grouted anchor system appeared to anchor the rods reliably even after subsequent loss of pressurization. The linear differential transformer type sensors provided a more than adequate displacement range and sensitivity and were essentially trouble-free. Only one of the 158 Teflon-sheathed thermocouples that were mounted on the extensometer rods failed, and that one exception was damaged at the time of installation. The temperature-versus-depth profiles generated from these thermocouples appeared to be normal except in the cases of three vertical extensometers that had become at least partially filled with water. Convection currents within the water column are thought to have produced the abnormal temperature profiles. Several horizontal extensometers also leaked, but those holes were inclined sufficiently off the horizontal to be self-draining. The seepage from these holes generated a maintenance problem when the water collected in the protective cover enclosing the sensors and their electrical terminals.

The most important steps that could be taken to improve the extensometers are: (1) reduce the hysteresis by reducing the sources of rod and head friction; (2) improve the downhole waterproofing system to eliminate the deleterious effects of corrosion; (3) improve the instrument calibration

scheme to more accurately reflect the response of the sensor to anchor displacement as opposed to head displacement; (4) eliminate the tendency of the sensor mount to loosen as a response to head vibration; and (5) provide a design that will eliminate any uncertainty in the sensor installation position.

Some steps that would improve the application of the instrument over that achieved at Stripa are: (1) cast a level concrete reference collar around each extensometer borehole to provide a convenient reference for depth measurements; (2) use a gas-over-oil accumulator in the anchor inflation system; (3) maintain a surveillance system to monitor the sensor power-supply voltage; (4) operate the sensors so that, over their required displacement, their output voltage will not pass through zero; (5) if the hysteresis problem has not been eliminated, provide an automatic head vibration system; and (6) exercise great care in eliminating the sources of electrical noise from the data collection system.

Two laboratory mock-ups of a horizontal extensometer provided considerable detail regarding the effect various parameters had upon the hysteresis of this instrument. The laboratory tests demonstrated that the hysteresis resulting from moving an anchor was considerably greater than that resulting from moving the head. We believe that the effect of friction in the head would be similar for vertical and horizontal extensometers and would be relatively independent of rod length. However, for downhole friction, the effect would be greater for horizontal extensometers, for longer rods, and for rods that pass through a greater number of intervening anchors. As part of the laboratory work, a device, which we

have called a microadjuster, was developed to perform field calibration more rapidly and in such a way that the hysteresis that is frictionally stored in (or near) the head of an extensometer could be evaluated.

The correction for thermal expansion of the Superinvar rods, even when operated over a modest temperature range, was shown to be a critical element in evaluating the net displacement of an anchor. In one case, this thermal correction was larger than the gross indicated displacement, even though no part of the rod exceeded 80°C. This problem in obtaining a high degree of accuracy in the differences between two measured displacements is inherent in any case where the thermal corrections are of the same order of magnitude as the indirect displacements of the individual rods.

These observations emphasize the need for especially careful calibration and mounting of thermocouples as well as accurate evaluation of the expansion characteristics of the rod material. If possible, thermocouples should be mounted so that they can be removed for recalibration. If at least one thermocouple is installed inside a plastic guide tube, a full vertical temperature survey can be made along the longest rod. The output of this sensor could be used to verify the accuracy of the temperature interpolation algorithm.

Because the measured displacements were relatively small (maximum excursion 3.1 mm and typical excursion less than 0.5 mm) and because the proposed analysis of the thermomechanical response of the rock requires a knowledge of the differences between these small values, measurement accuracy was of paramount importance. Early in the experiment, a stepwise

output from the extensometers that would seriously reduce the usefulness of the data was observed. Laboratory tests demonstrated that friction within the instrument could be responsible for as much as 184 μm of hysteresis in the indicated displacement. A field test at Stripa demonstrated that this friction was responsible for a stepwise output of as much as 81 μm which could be released by rapping the head assembly. As a result of these observations, a daily routine was instituted in which each extensometer head was vibrated to release any frictionally stored rod displacement. This procedure transformed the stepwise response into a relatively smooth output.

8. ACKNOWLEDGMENTS

This project was sponsored by the U.S. Department of Energy through the Office of Nuclear Waste Isolation, Battelle Memorial Institute, under Contract DE-AC03-76SF00098. M.R. Wigley acted as project manager for the Office of Nuclear Waste Isolation. His support for the work is gratefully acknowledged.

We also wish to thank P.H. Nelson for his support and insightful suggestions throughout the course of this work. B. Boisen of Terrametrics, Inc. provided many helpful discussions regarding the original design and manufacture of these instruments, as well as assistance in locating other sources of detailed information regarding the materials of construction. T.H. Schrauf and R. Lingle of Terra Tek Inc. provided information regarding the initial field installations. H. Carlsson designed the rod-puller tool and supervised its initial application. R. Galbraith and H. Sellden performed field tests and monitored the operation of the extensometers. S.A. Lundgren designed the apparatus for the laboratory mock-up tests and assisted with the operation of the tests.

9.0 REFERENCES

Binnall, E.P., and M.B. McEvoy, 1981. Assessment of Thermocouple Temperature Measurement During In-Situ Heater Experiments at Stripa, Sweden. LBL-12670, Lawrence Berkeley Laboratory Report, University of California, Berkeley, California (in preparation).

Binnall, E. P., A.O. DuBois, and R. Lingle, 1979. "Rock Instrumentation Problems Experienced During In situ Heater Tests," presented at the International Symposium on the Scientific Basis for Nuclear Waste Management, Materials Reserarch Society, Boston, Ma., Nov. 27-30, 1979. LBL 9952, Lawrence Berkeley Laboratory, University of California, Berkeley, California.

Burleigh, R.H., E.P Binnall, A.O. DuBois, D.O. Norgren, and A.R. Ortiz, 1979. Electrical Heaters for Thermo-mechanical Tests at the Stripa Mine. LBL-7063, (SAC-13) Lawrence Berkeley Laboratory, University of California, Berkeley, California.

Chan, T., E. Binnall, P. Nelson, O. Wan, C. Weaver, K. Ang, J. Braley, and M. McEvoy, 1980. Thermal and Thermomechanical Data from In Situ Heater Experiments at Stripa, Sweden. LBL-11477, (SAC-29) Lawrence Berkeley Laboratory, University of California, Berkeley, California.

Hood, M., 1979. "Some Results from a Field Study of Thermo-mechanical Loading of a Rock Mass when Heater Canisters are Emplaced in the Rock," 20th Symposium Rock Mechanics, Austin, Texas, pp. 429-438; LBL-9392 (SAC-26) Part I., Lawrence Berkeley Laboratory, University of California, Berkeley, California.

International Nickel Company, 1962. Iron-Nickel and Related Alloys of the Invar and Elinvar Types (30% to 60% Nickel).

Kurfurst, P.J., T. Hugo-Persson, and G. Rudolph, 1978. Borehole Drilling and Related Activities at the Stripa Mine. LBL-7080, (SAC-05) Lawrence Berkeley Laboratory, University of California, Berkeley, California.

McEvoy, M.B., 1979. Data Acquisition, Handling, and Display for the Heater Experiments at Stripa. LBL-7062 (SAC-14) Lawrence Berkeley Laboratory, University of California, Berkeley, California.

Lingle, R., P.H. Nelson, A. DuBois, and H. Sellden, 1984. Performance of Borehole Deformation Gauges and Vibrating Wire Stressmeters at Stripa. LBL 13327, Lawrence Berkeley Laboratory, University of California, Berkeley, California.

Nelson, P.H., R. Rachiele, J.S. Remer, and H.S. Carlsson, 1981. Water Inflow into Boreholes During the Stripa Experiments. LBL-12547 (SAC-35) Lawrence Berkeley Laboratory, University of California, Berkeley, California.

Schrauf, T.A., H. Pratt, E. Simonson, W. Hustrulid, P. Nelson, A. DuBois, E. Binnall, R. Haught, 1979. Instrumentation Evaluation, Calibration and Installation for the Heater Experiments at Stripa. LBL-8313, (SAC-25) Lawrence Berkeley Laboratory, University of California, Berkeley, California.

Terrametrics Incorporated, 1977. Data Acquisition System Calibration, Job #6499, August 31, 1977

Witherspoon, P.A. and O. Degerman, 1978. Swedish-American Cooperative Program on Radioactive Waste Storage in Mined Caverns -- Program Summary. LBL-7049 (SAC-01) Lawrence Berkeley Laboratory, University of California, Berkeley, California.

APPENDIX A:

LABORATORY TEST DATA

All laboratory test data from the second extensometer mock up is presented in graphical form. The symbols and format are defined on Figure 22. One division on either the abscissa (anchor displacement) or the ordinate (sensor response) is equal to 100 μm. All of the graphs on one page are for a given set of test parameters. The letter identifies the particular set of parameters as defined in Table 9. The number identifies a particular anchor, rod, and sensor.

1 = sensor on 3 meter long rod from anchor No. 1

2 = sensor on 6 meter long rod from anchor No. 2

3 = sensor on 9 meter long rod from anchor No. 3

4 = sensor on 12 meter long rod from anchor No. 4.

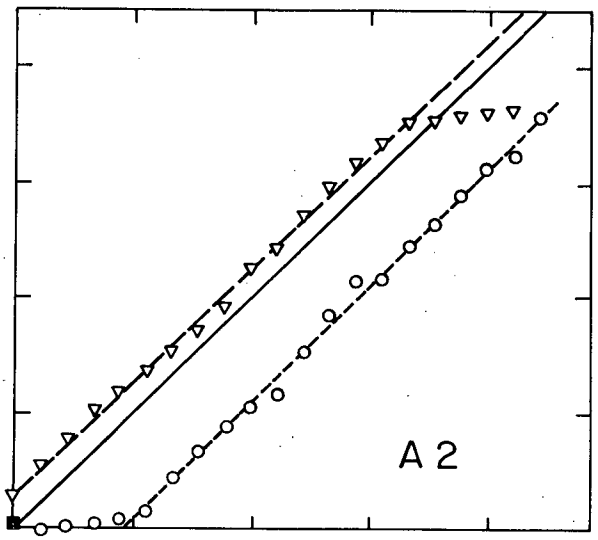

XBL 847-2756

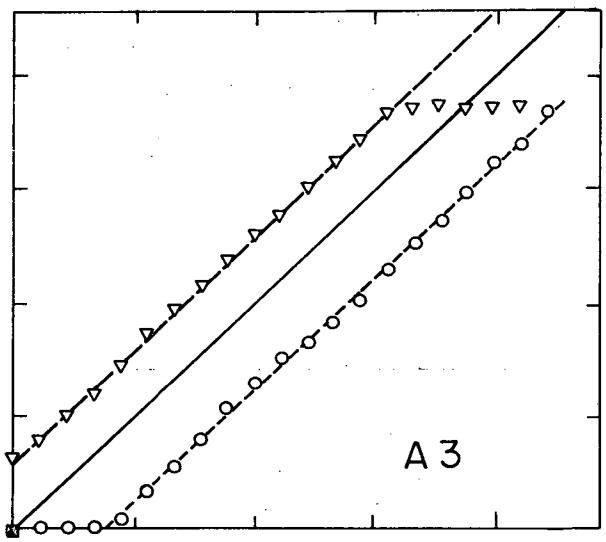

XBL 847-2757

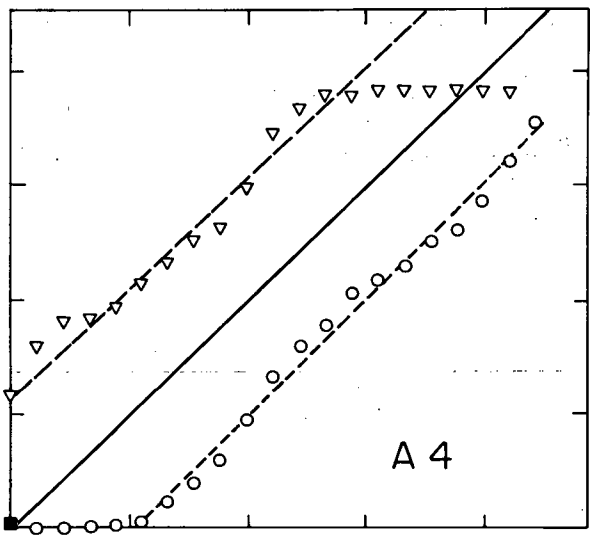

XBL 847-2758

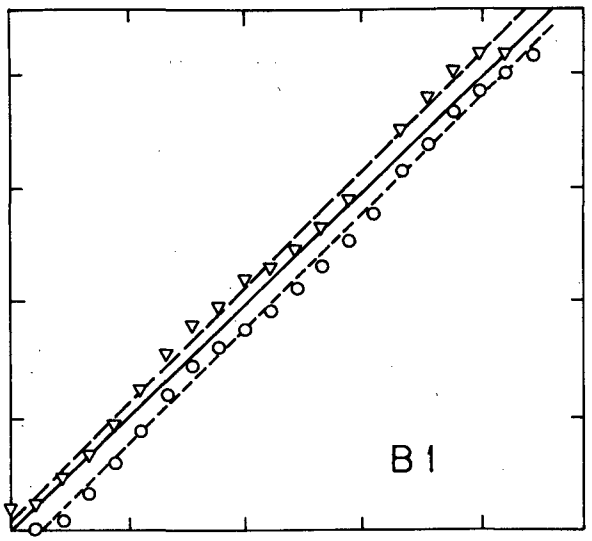

XBL 847-2759

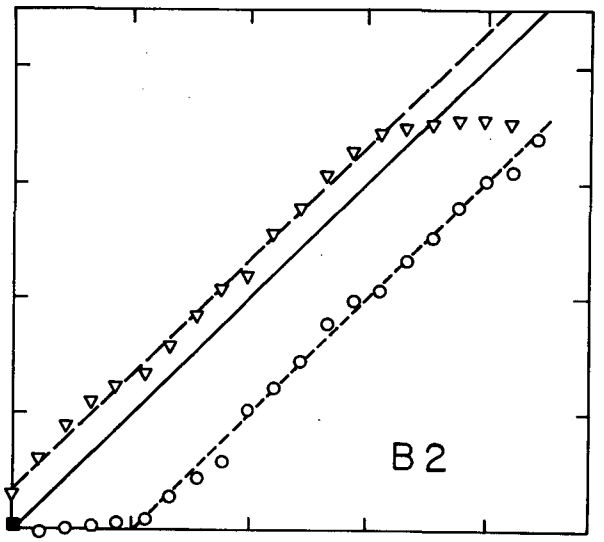

XBL 847-2760

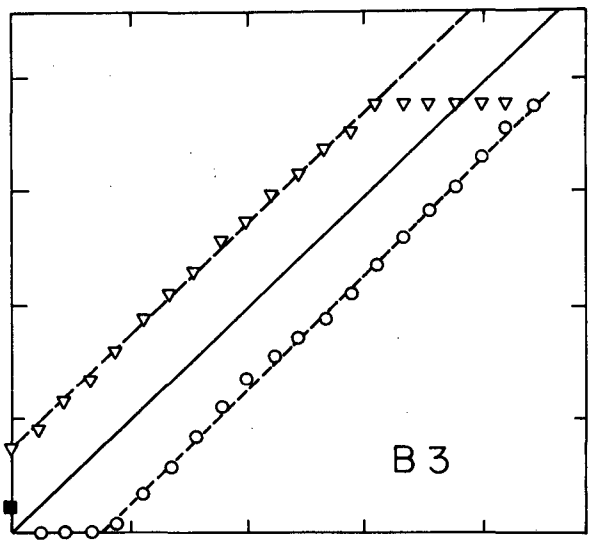

XBL 847-2761

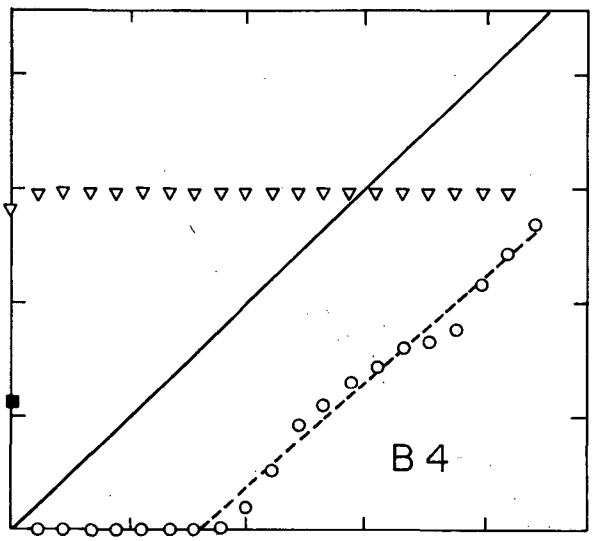

XBL 847-2762

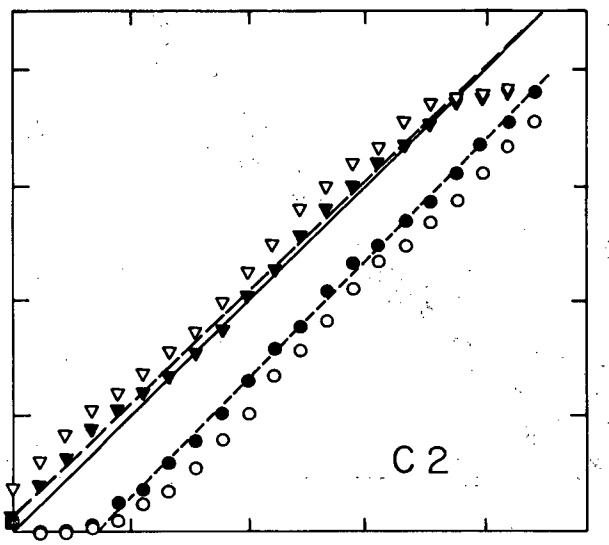

XBL 847-2763

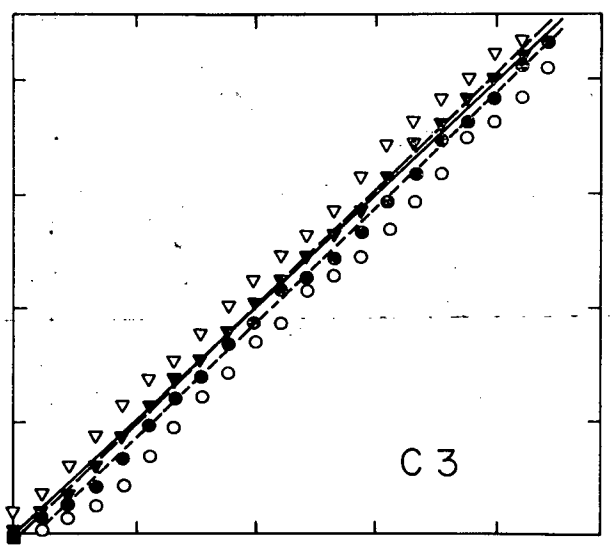

XBL 847-2764

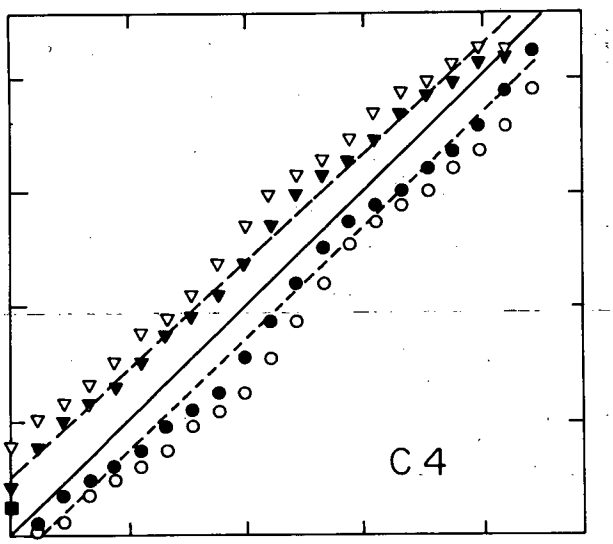

XBL 847-2765

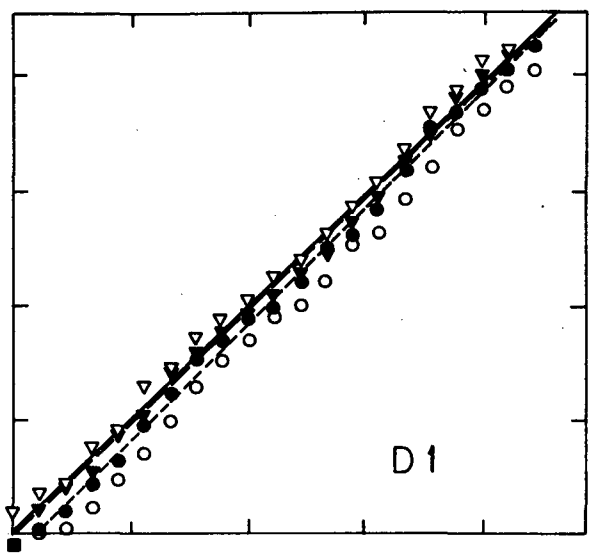

XBL 847-2766

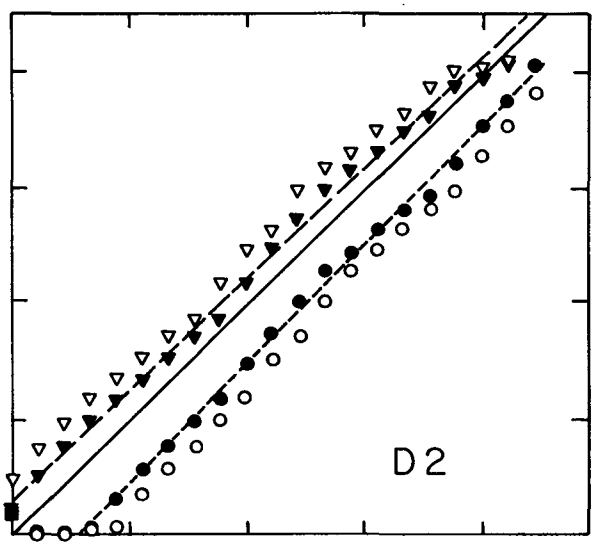

XBL 847-2767

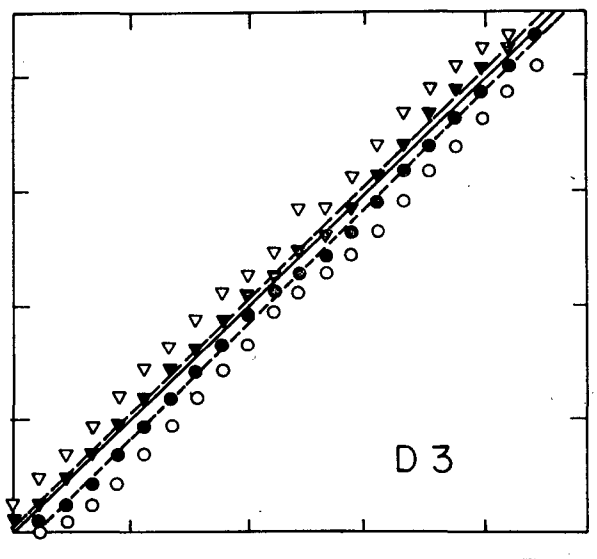

XBL 847-2768

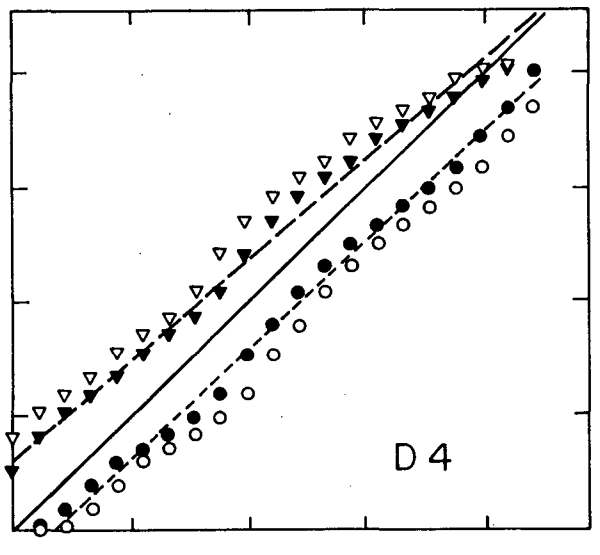

XBL 847-2769

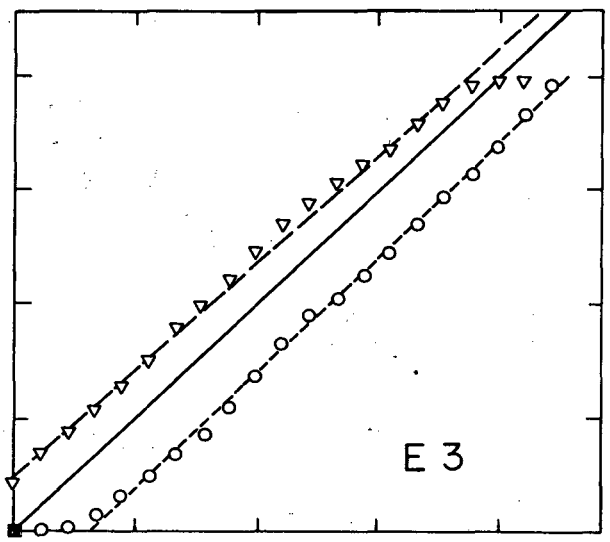

XBL 847-2770

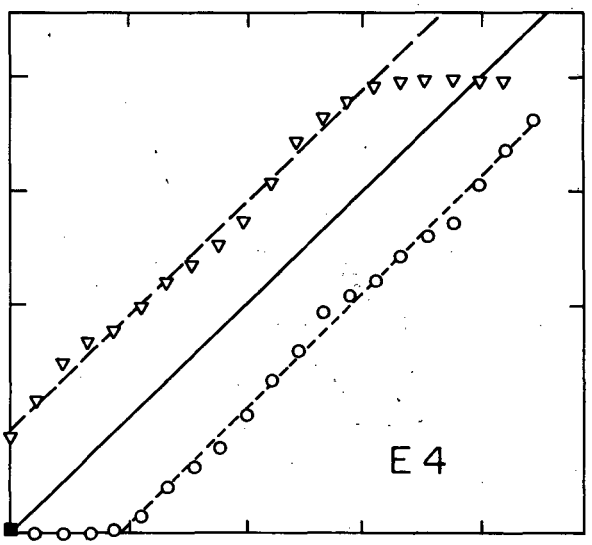

XBL 847-2771

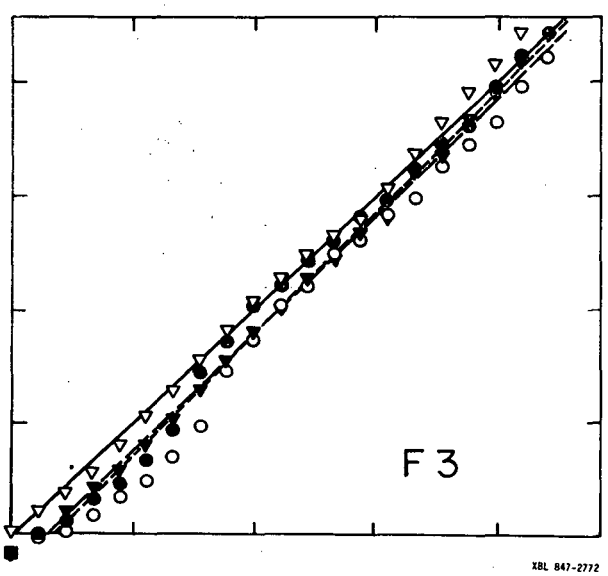

XBL 847-2772

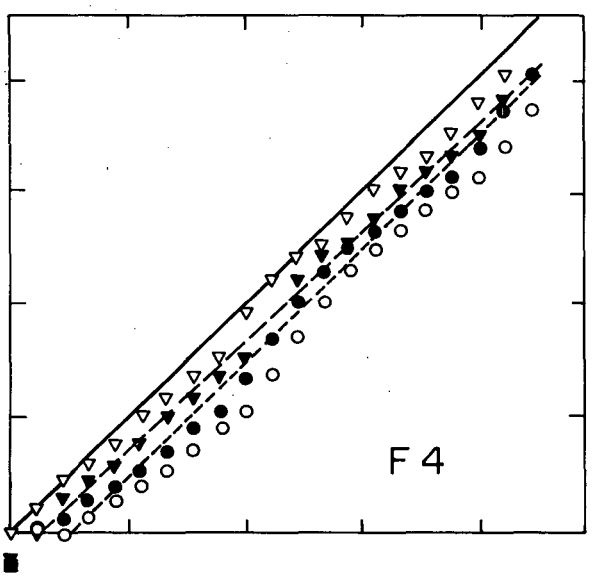

XBL 847-2773

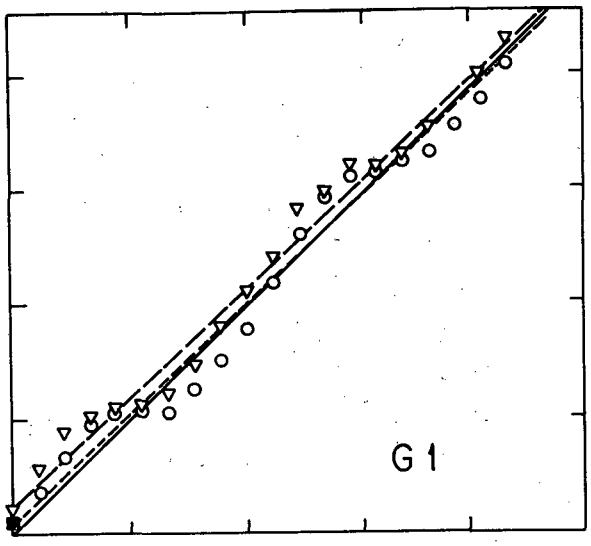

XBL 847-2774

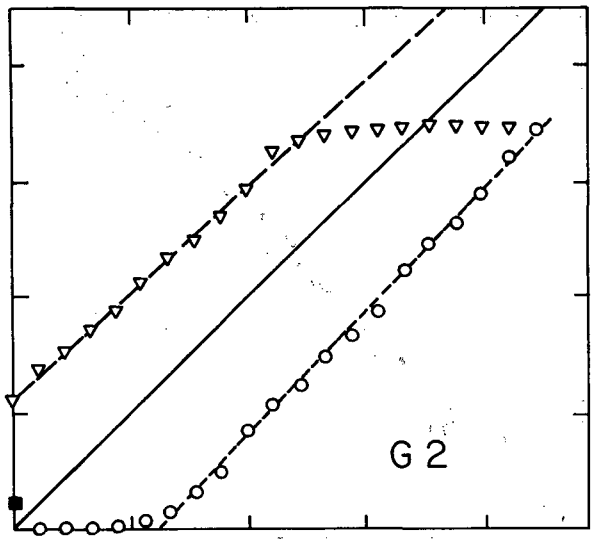

XBL 847-2775

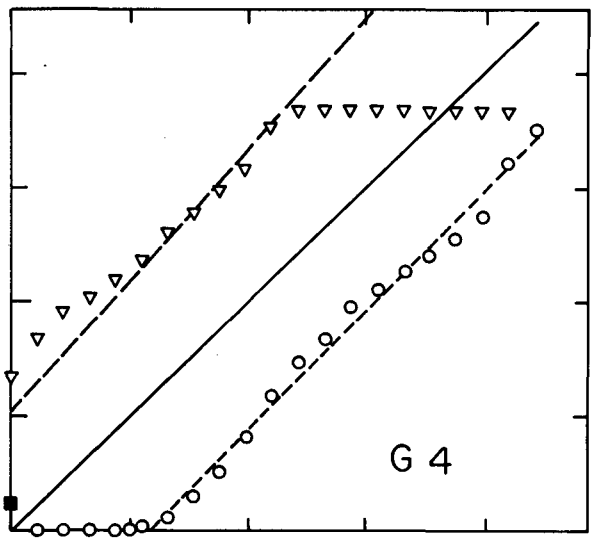

XBL 847-2776

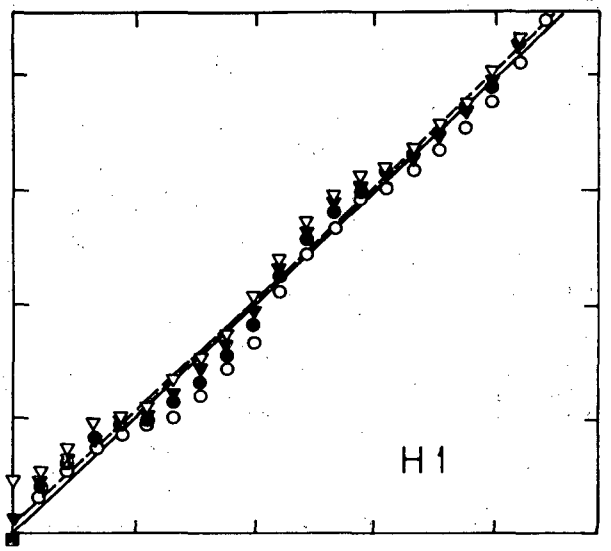

XBL 847-2777

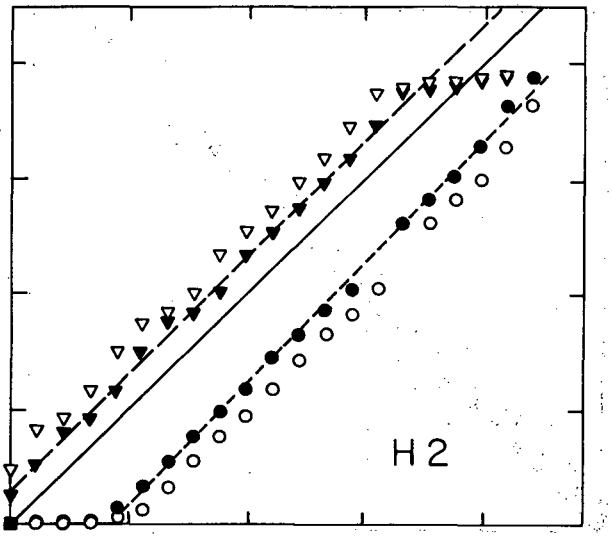

XBL 847-2778

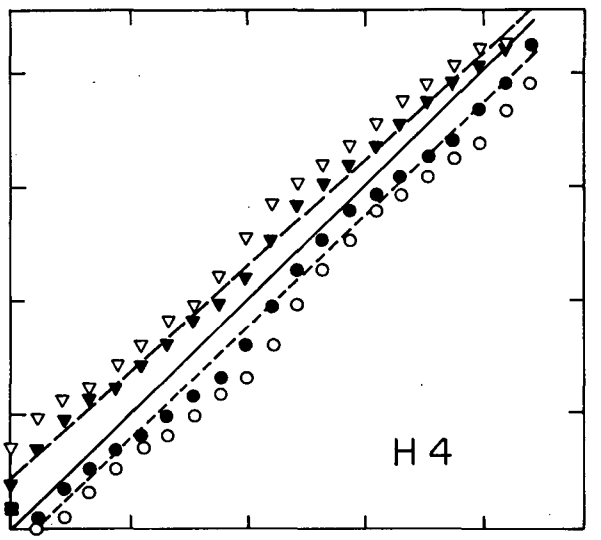

XBL 847-2779

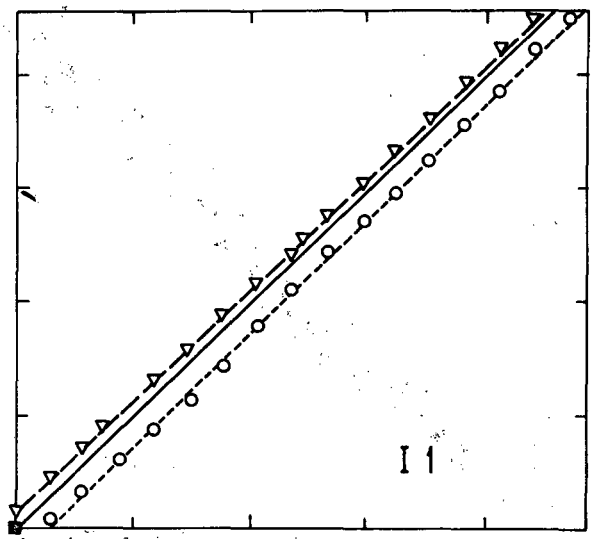

XBL 847-2780

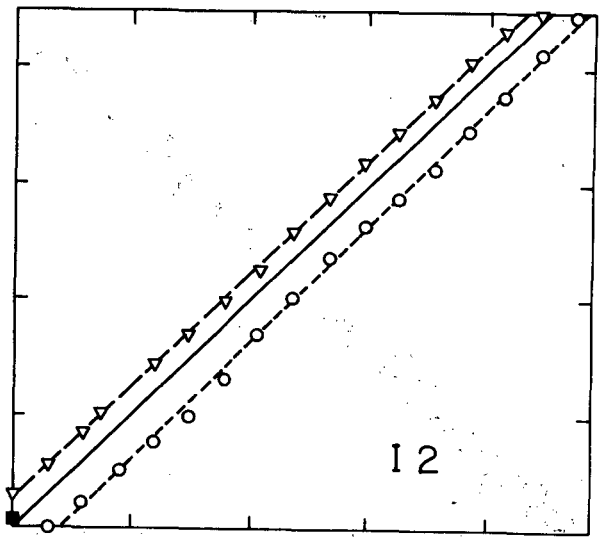

XBL 847-2781

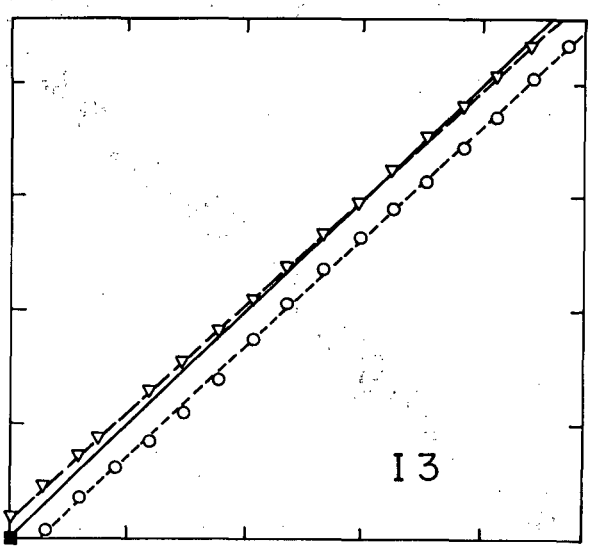

XBL 847-2782

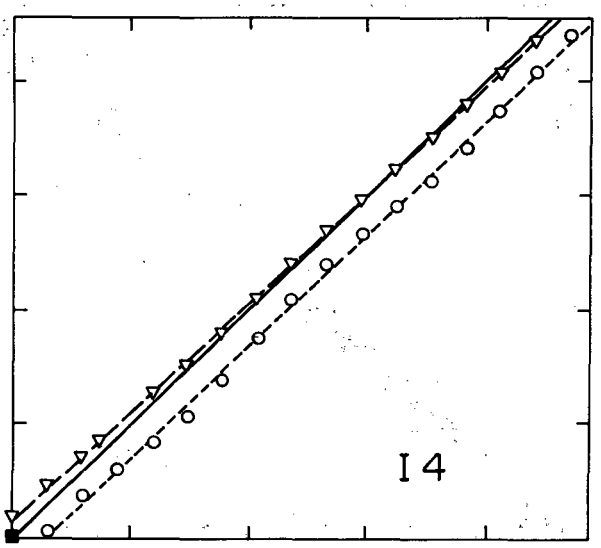

XBL 847-2783

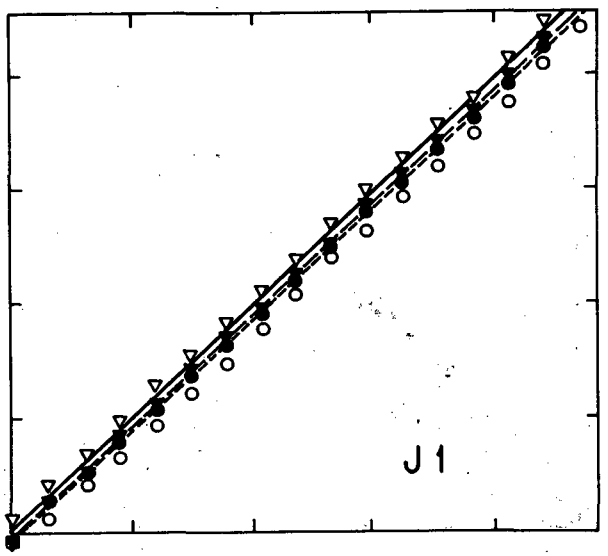

XBL 847-2784

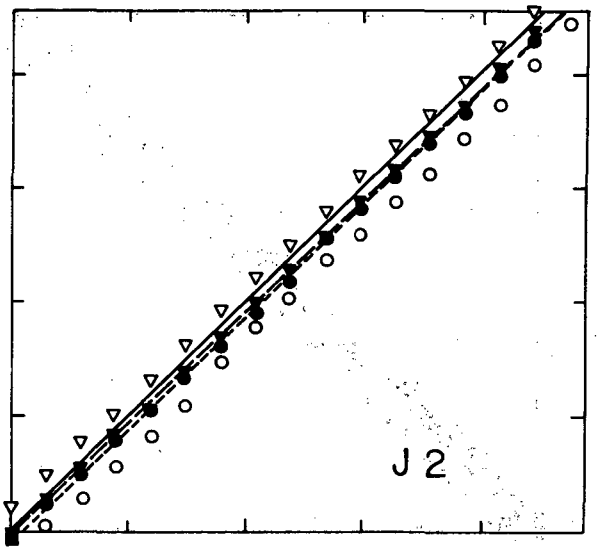

XBL 847-2785

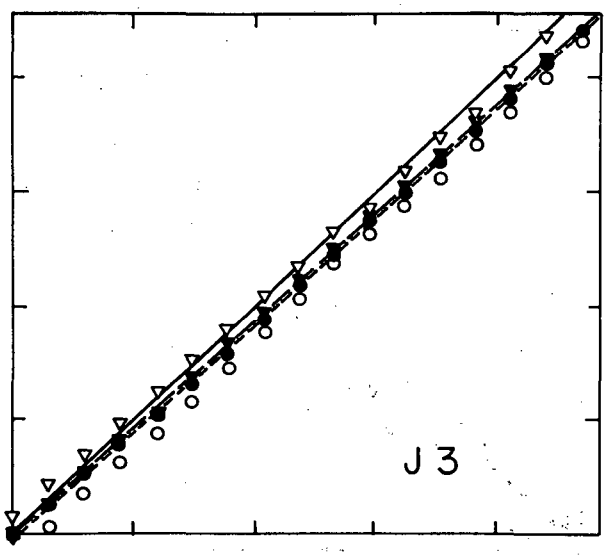

XBL 847-2786

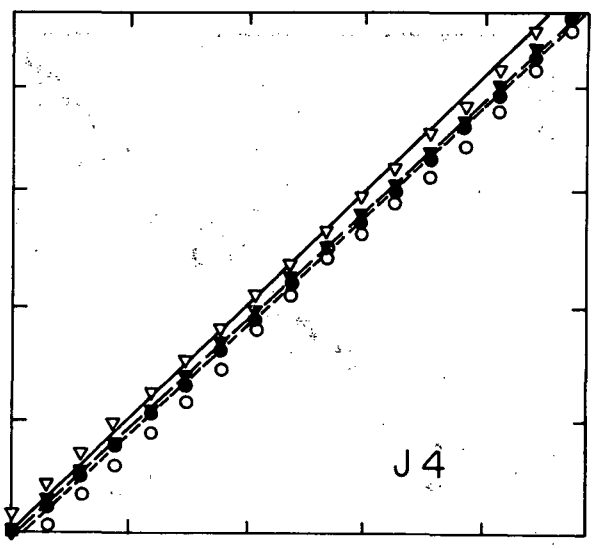

XBL 847-2787

This report is part of a cooperative Swedish-American project supported by the U.S. Department of Energy and/or the Swedish Nuclear Fuel Supply Company. Any conclusions or opinions expressed in this report represent solely those of the author(s) and not necessarily those of The Regents of the University of California, the Lawrence Berkeley Laboratory, the Department of Energy, or the Swedish Nuclear Fuel Supply Company.

TECHNICAL INFORMATION DEPARTMENT
LAWRENCE BERKELEY LABORATORY
UNIVERSITY OF CALIFORNIA
BERKELEY, CALIFORNIA 94720